Chapter 3
Atmosphere–Ionosphere Electrodynamic Coupling

V.M. Sorokin and V.M. Chmyrev

Abstract Numerous phenomena that occur in the mesosphere, ionosphere, and the magnetosphere of the Earth are caused by the sources located in the lower atmosphere and on the ground. We describe the effects produced by lightning activity and by ground-based transmitters operated in high frequency (HF) and very low frequency (VLF) ranges. Among these phenomena are the ionosphere heating and the formation of plasma density inhomogeneities, the excitation of gamma ray bursts and atmospheric emissions in different spectral bands, the generation of ULF/ELF/VLF electromagnetic waves and plasma turbulence in the ionosphere, the stimulation of radiation belt electron precipitations and the acceleration of ions in the upper ionosphere. The most interesting results of experimental and theoretical studies of these phenomena are discussed below. The ionosphere is subject to the action of the conductive electric current flowing in the atmosphere–ionosphere circuit. We present a physical model of DC electric field and current formation in this circuit. The key element of this model is an external current, which is formed with the occurrence of convective upward transport of charged aerosols and their gravitational sedimentation in the atmosphere. An increase in the level of atmospheric radioactivity results in the appearance of additional ionization and change of electrical conductivity. Variation of conductivity and external current in the lower atmosphere leads to perturbation of the electric current flowing in the global atmosphere–ionosphere circuit and to the associated DC electric field perturbation both on the Earth's surface and in the ionosphere. Description of these processes and some results of the electric field and current calculations are presented below. The seismic-induced electric field perturbations produce noticeable effects in the ionosphere by generating the electromagnetic field and plasma disturbances. We describe the generation mechanisms of such experimentally observed effects as excitation of plasma density inhomogeneities, field-aligned

V.M. Sorokin (✉)
Pushkov Institute of Terrestrial Magnetism, Ionosphere and Radio Wave Propagation, Russian Academy of Sciences, IZMIRAN, Troitsk, Moscow Region 142190, Russia

V.L. Bychkov et al. (eds.), *The Atmosphere and Ionosphere*,
Physics of Earth and Space Environments,
DOI 10.1007/978-90-481-3212-6_3,

currents, and ULF/ELF emissions and the modification of electron and ion altitude profiles in the upper ionosphere. The electrodynamic model of the ionosphere modification under the influence of some natural and man-made processes in the atmosphere is also discussed. The model is based on the satellite and ground measurements of electromagnetic field and plasma perturbations and on the data on atmospheric radioactivity and soil gas injection into the atmosphere.

Keywords Electromagnetic field · Plasma disturbances · Upper ionosphere · Atmosphere

3.1 Introduction

This chapter presents a review of the most interesting results of experimental and theoretical studies of the electromagnetic field and plasma disturbances in the ionosphere, which are initiated by different natural sources in the atmosphere and on the ground, and of the technogenic disturbances connected with human activity. A chain of interconnected processes in the lithosphere–atmosphere–ionosphere interaction system causes the ionosphere to react on such phenomena as earthquakes, volcano eruptions, typhoons, lightning discharges, high power explosions, functioning of powerful sources of electromagnetic radiation, etc. Due to such coupling, the ionosphere appears to be a sensitive indicator of the many processes occurring on the ground and in the near-Earth atmosphere. Apparently, this factor defines growing interest to investigation of the atmosphere–ionosphere interaction.

A fundamental role in the energy transfer from the atmosphere to the ionosphere belongs to thunderstorms. Large quasi-electrostatic fields in the mesosphere and the lower ionosphere connected with cloud-to-ground lightning discharges and intense electromagnetic pulses of ∼20 GW peak power generated by lightning current cause significant ionospheric disturbances because of the heating and acceleration of electrons, production of ionization, optical emissions, gamma ray bursts, etc.

Other powerful mechanism of lightning influence on the ionosphere is connected with additional ionization and formation of ionospheric inhomogeneities that are caused by the radiation belt electron precipitation due to the pitch-angle scattering of trapped particles in the magnetosphere by whistler mode waves from lightning.

Technogenic effects in the ionosphere also became a subject of intense experimental and theoretical studies. Significant attention is devoted to controlled influence on the ionosphere aimed at generating the desired ionospheric response dependent on the parameters of influence. In this connection, one can mention the generation of ultra low frequency (ULF)/extra low frequency (ELF) waves in a process of ionosphere heating by the radiation of powerful high frequency (HF) transmitters [1–4], the formation of artificial very low frequency (VLF) ducts and other types of inhomogeneities [5–7], the acceleration of ions and the excitation of atmospheric emissions in different spectral bands [8–11], etc. One can note the

transition into an active phase of the investigation of VLF wave impact on the high-energy particle distributions in the Earth's radiation belt including the experiments that use powerful VLF transmitter onboard spacecraft [12,13].

Since physical mechanisms for transfer of perturbations into the ionosphere from the abovementioned natural and artificial sources in many cases are similar, we thought it reasonable to discuss both types of influence (natural and man-made) in a frame of one paper. Such phenomena as the effects of ballistic rocket launches and of explosions of different kinds on the ionosphere stand by itself. These effects are of a different physical nature, and, therefore, their consideration lies beyond the scope of this chapter.

Among the numerous natural sources influencing the ionosphere, the most important role is thought to be played by earthquakes. An importance is defined by the potential of using the ionosphere as a sensitive indicator of earthquake preparation processes and possible tool for the short-term earthquake forecasting in future. Such potentiality is based on numerous ground and satellite observations of seismic-related phenomena occurring in the atmosphere and the ionosphere of the Earth several days or weeks before earthquake. Some results of these observations are reviewed in refs. [14–17]. Though the number of publications devoted to seismic effects on the ionosphere is huge, there is no more or less complicated understanding of cause–effect relations between the phenomena involved in the ionosphere responding to the seismic processes. Because of the insufficient experimental base and a lack of reliable statistical data on the ionospheric precursors to earthquakes, currently, there is no tangible ground to use ionospheric phenomena for sure earthquake forecasting. Nevertheless, a noticeable progress comes to pass in accumulating and analyzing the data from satellite and ground-based observations and in theoretical modeling of interconnected processes in the lithosphere–atmosphere–ionosphere system. Significant contribution is done from the Demeter satellite research program (see, e.g. [18–20]). A comprehensive model of the lower atmosphere and the ionosphere coupling was developed in ref. [21].

We can suppose that the earthquake effects in the ionosphere arise as a result of simultaneous actions of various factors, such as acoustic waves, electric fields, electromagnetic radiation, chemically active substances, etc. Since seismic activity is accompanied by the enhanced injection of soil aerosols into the atmosphere, an important role in the formation of these factors is played by aerosol fluxes, which influence the electric conductivity and generate external electric currents in the lower atmosphere [22]. Experimental evidences of earthquake-related enhancement in the injection of soil aerosols into the atmosphere, the increase in concentration of some gases (e.g., H_2, CO_2, and CH_4) by several orders of magnitude in seismically active zone, and the increase in atmospheric radioactivity associated with such radioactive elements as radon, radium, uranium, thorium, and actinium and their decay products on the eve of earthquake are presented in refs. [23–28]. Effects of strong atmospheric processes associated with typhoons on the electric field and plasma density fluctuations in the ionosphere were reported in refs. [29, 30].

Satellite measurements carried out during last 2 decades (see, e.g., [18, 20, 31, 32] confirmed the existence of low frequency emissions associated with earthquakes,

which was first reported by [33]. Comparison of the ground-based observations and the satellite measurements of ELF waves performed during different seismic events showed the similarity of the observed emissions; the only difference was in the wave intensity in the ionosphere and on the ground [34]. The negative experimental findings in [35] were connected with the use of incorrect method for data reduction: short events ($\leq$ 5 s), such as single or a small number of spherics or whistlers were not classified as disturbances and were hence not considered. At the same time, the ELF precursors to earthquakes could be associated with thunderstorm electromagnetic pulses propagated in the Earth–ionosphere waveguide and scattered into the ionosphere by plasma inhomogeneities formed in the lower ionosphere over the seismic zone before an earthquake [36]. The duration of such pulses is much less than 2 s, and the maximum power is concentrated at frequencies below $\sim$500 Hz.

DC electric field perturbations can play a key role in a coupling between the lower atmosphere and the ionosphere [21]. Ground-based and satellite observations confirm an enhancement of the electric field both in the ionosphere and on the ground in a seismic zone before earthquakes [37–42].

Small-scale plasma irregularities and large-scale disturbances of electron and ion density profiles in the upper ionosphere over seismically active region were observed before earthquakes [28, 32, 43–46].

The formation of thermal anomalies in seismic zones several days before large magnitude earthquakes presents another pronounced effect that is well observable from satellites with the use of IR sensors [47–50]. In addition, we can mention the observations of anomalous airglow at 557.7 and 630 nm correlated with the growth of seismic activity [51].

Numerous theoretical models were suggested for explanation of separate phenomena stimulated in the atmosphere and the ionosphere by seismic activity. Reference [52] considered the generation and propagation of internal gravity waves and their effects on the ionosphere. The generation of ULF emissions by lithospheric sources and their possible penetration into the ionosphere was analyzed in refs. [53–55]. The formation of electric currents in the lithosphere and the propagation of the excited waves from the source region into the ionosphere were considered in refs. [56,57]. Possible acoustic effects on the ionosphere and the generation of geomagnetic pulsations were investigated in refs. [38, 58, 59] considered the conductivity and the electric field variations in the lower atmosphere that can be caused by increase in radon concentration connected with the growth of seismic activity. The enhanced injection of radon and metallic aerosols in the epicenter region and its influence on the ionosphere were discussed in ref. [28]. The mechanisms for the electric field penetration from the source region in the lithosphere into the ionosphere and related effects on the ionosphere were analyzed in refs. [60,61].

Electrodynamic model of the ionosphere response to seismic-related lower atmosphere disturbances is developed in ref. [22]. This model describes the complete chain of processes in the lithosphere–ionosphere coupled system, which starts from the injection of radioactive substances and charged aerosols into the atmosphere and the formation of external electric current. This current is responsible for

the enhancement of DC electric field and the subsequent development of acoustic-gravity wave (AGW) instability in the ionosphere. It results in the generation of conductivity inhomogeneities in the lower ionosphere, the formation of magnetic field-aligned currents and plasma density disturbances in the upper ionosphere stretched along geomagnetic field lines. Besides, the electric field increase leads to an additional Joule heating of the lower ionosphere, which results in an elevation of F-layer maximum, a decrease of electron density in the maximum of this layer, and a growth of light ion density in the upper ionosphere. Thus, this model connects disturbances of the electric field and the key ionosphere parameters with increase of atmospheric radioactivity and injection of charged aerosols into the ionosphere. Detailed consideration of all these processes is presented below.

3.2 Effects of Lightning and Powerful Ground-Based Transmitters on the Near-Earth Space

3.2.1 Lightning Effects on the Ionosphere and the Magnetosphere

Thunderstorms play a fundamental role in the energy transfer from the atmosphere to the ionosphere. At any given time, more than 2,000 thunderstorms are active over the globe, and on average, lightning strikes the Earth about 100 times per second [62]. Every cloud-to-ground lightning discharge transfers to the ground a charge of the order of ~300 C during several milliseconds, leading to the formation of large quasi-electrostatic fields in the mesosphere and the lower ionosphere over millisecond time scales [63]. These fields together with intense electromagnetic pulses of ~20 GW peak power generated by lightning current [64] cause significant disturbances in the lower ionosphere due to heating of the ambient electrons and acceleration of runaway electrons, producing ionization and optical emissions [63, 65–67].

Plasma inhomogeneities caused by high-energy electron precipitation from the Earth's radiation belt in a process of pitch-angle scattering of trapped particles by intense whistler mode waves from lightning discharges present other class of lightning-induced disturbances in the ionosphere. Troposphere–magnetosphere coupling of such kind has been many times confirmed in ground-based observations [68–70], balloon measurements [71], rocket experiments [72, 73], and satellite observations [74–76]. Theoretically, the mechanism of pitch-angle scattering and particle precipitation from the radiation belt by ducted whistlers in the magnetosphere is also well investigated (see, e.g. [77, 78] and references therein).

Experimental indication of strong electrodynamic coupling of thunderstorms to the mesosphere and the lower ionosphere includes such phenomena as fast lightning-induced perturbations of subionospheric VLF transmitter signals propagating over the thunderstorm areas [79–84], optical emissions associated with sprites [85–91] and blue jets [92], and airglow enhancements [93] connected with

short-term (<1 ms) "elves" emissions excited at 80–95 km altitudes before sprites [65, 88, 94]. Sprites clearly associated with intense lightning discharges [95] are correlated with fast perturbations of subionospherically propagating VLF signals [82], providing an evidence of interconnection of these phenomena. An important manifestation of strong upward energy pumping from thunderstorms was obtained from the observations of gamma-ray flashes of atmospheric origin [96] associated with lightning discharges [97] and of intense bursts of broadband VHF emissions [98].

The existing generation models of the abovementioned phenomena are based on heating of the ambient electrons by electromagnetic pulses from lightning discharges [65, 99–102] or by quasielectrostatic thundercloud electric fields [103–106], and on runaway electron acceleration processes [107–109].

First registration of optical emissions stimulated by lightning has been reported by Franz et al. in ref. [110]. Later, numerous observations of similar flashes of luminescence called sprites [111] have been performed from the ground [86, 90, 91], the aircraft [92, 111–113], and space-based platforms [89,114]. The main characteristics of sprites obtained from these measurements could be summarized as follows. This phenomenon is usually observed at 50–90 km altitudes over positive cloud-to-ground lightning discharge with peak current of the order of 100 kA or above. Transverse size of luminescence area is 5–50 km; sometimes containing structural elements with a cross section of ~2 km. Sprite arises 1.5–4 ms after lightning discharge and lasts for several milliseconds. The brightness of sprites was estimated to be 25–50 kR, for most intense events it was up to 100 kR. Maximum of intensity ranges between spectral bands 650–680 nm and 750–780 nm.

Blue jets present other type of luminescence occurring at altitudes below 50 km over thunderstorm clouds. They are observed as narrowly collimated light beams of blue color propagating upward from thunderclouds with velocity ~100 km/s up to 40–50 km altitudes, where they disappear. Blue jets in contrast to sprites are not accompanied by strong electromagnetic radiation in VLF range. Observations did not display direct connection with simultaneous cloud-to-ground lightning discharges [115]. Blue jet generation theory based on accumulating charges in thundercloud and subsequent breakdown ionization and upward propagation of ionization wave has been developed by Pasko et al. in ref. [105].

Electron heating in the lower ionosphere by the thundercloud's electric field can lead to enhancement of infrared radiation, particularly to intensification of CO_2 emission at 4.3 μm wave length [116]. Different electromagnetic emissions associated with thunderstorm activity have been observed onboard the Demeter satellite [117]. The effects of ion heating and generation of plasma turbulence in the ionosphere under the influence of lightning discharges were reported by Berthelier et al. in ref. [118] based on the Demeter data.

As mentioned above, one of important mechanisms of the troposphere–ionosphere–magnetosphere coupling is lightning-induced precipitation of high energy (>40 keV) electrons from the Earth's radiation belt into the ionosphere [76, 119, 120]. Comprehensive data of satellite observations of this phenomenon were reported by Voss et al. [76], who used the low orbital (170–280 km) S81-1

polar satellite measurements of electron and ion fluxes with energies 2–1,000 keV and 10–1,500 keV, respectively. These observations were accompanied by the ground wave measurements at Palmer station in Antarctica. Analysis of numerous precipitation events associated with lightning has shown that the time delay between causative spheric and appearance of first burst of precipitating particles registered on satellite increased with L-shell according to prediction of theory [78]. The global distribution of intense precipitations of such kind correlated with thunderstorm activity distribution and displayed maximum in the depletion zone of the electron radiation belt at $2 < L < 3$. The density of electron energy flux in lightning-induced precipitations was about $\sim 10^3$ erg·cm^{-2}·s^{-1} (10^{-4} J/(m^2 s)) and particles with an energy of 100–200 keV prevailed. The most recent experimental data on electron precipitations stimulated by lightning were obtained from the Demeter satellite [121]. Bursts of 100–300 keV electrons registered within 1s after an arrival of causative VLF pulses from lightning were observed.

3.2.2 *Effects of the Ionosphere Heating by Powerful HF Transmitters*

The first successful observations of the lower ionosphere heating by electromagnetic radiation from a powerful ground-based HF (3–30 MHz) transmitter were carried out in ref. [122]. They used the experimental HF transmitter in Platteville, Colorado, 50 MW effective isotropic-radiated power, as a heater and subionospheric VLF (20 kHz) and LF (60 kHz) probe signals for detecting lower ionosphere heating by measurements of amplitude and phase perturbations in these signals. Transmissions were made at 5.1 and 7.4 MHz to heat the midday *D*-region and the diameter of the heated region at the reflection height of probe waves ($\sim$70 km) was $\sim$25 km. The heating effect in this region was obtained from the amplitude perturbation $\sim$0.53% (0.046 dB) at 60 kHz and phase perturbation $\sim 0.3^\circ$ at a frequency of 20 kHz.

Later, subionospheric VLF probe waves were used to probe *D*-region heating in the experiments by Barr et al. in refs. [123, 124] with steerable heater in Tromso (Norway) operated at the frequency of 2.759 MHz; the maximum effective radiated power was 200 MW. VLF probe waves were from the 12.1 kHz Omega navigation transmitter in Aldra, Norway, and the 16.4 kHz JXN transmitter nearby Helgeland. The heated spot was located near the end of <500 km great circle paths from the transmitters and had a form of a 27 by 34 km ellipse at 80 km height since the heating wave beam was focused on the Omega probe wave path (38° from vertical). Amplitude and phase perturbations of sub-ionospheric signals were correspondingly $\sim$0.05 dB and 0.3° during the daytime heating and up to 6 dB and 50° at night.

The heating experiment with the use of 2.8 MHz HIPAS transmitter near Fairbanks, Alaska, and 23.4 kHz probe waves from NPM transmitter in Oahu received at Fort Yukon, Alaska has demonstrated the perturbations in NPM amplitudes of -0.2 to $+0.4$ dB simultaneous with heater modulation patterns [125].

Beginning practically from earlier experiments, the lower ionosphere heating by intense modulated HF radiation in the presence of natural ionospheric electric currents (auroral electrojet and middle latitude dynamo currents) was investigated as a possible tool for the generation of electromagnetic ULF/ELF/VLF waves [1, 4, 126–131]. The generation mechanism is relatively simple. Periodic heating of the ionosphere in the current region modulates the electrical conductivity in this region and consequently causes the modulation of natural electric current. This process forms giant radiating antenna at the altitudes of 60–100 km. The generation of ULF/ELF/VLF waves by such antennas is extensively studied with the use of special high-frequency (HF) heating facilities in Tromso (Norway), Arecibo (Puerto Rico), HIPAS (High-Power Auroral Stimulation), and HAARP (High-frequency Active Auroral Research Program) (Alaska) and SURA (Russia). The most interesting results of these studies are presented below.

HF heater in Tromso operated at the frequencies from 2.7 to 8.0 MHz. A successful generation of ELF/VLF waves was carried out with the use of amplitude modulation by rectangular pulses in the frequency range 0.2–6.5 kHz. Maximum amplitudes of generated waves ~1, 0.1, and 0.03 pT were registered at the distances of 20, 200, and 500 km from the HF transmitter correspondingly [124, 126]. Successful excitation of the Earth–ionosphere waveguide and reception of artificially generated ELF/VLF signals with amplitude ~10 fT at the distance ~2,000 km has been demonstrated in several transmissions [129].

Amplitude measurements at large distances were used to estimate the power of ELF/VLF radiation from the ionosphere. Far-zone ground-based measurements have shown the amplitudes corresponding to ~1 W dipole radiation source at the altitude of maximum modulation of Hall conductivity in the ionosphere [124]. However, the satellite measurements [2] over the same heating facility have given an estimate of ~30 W for the ionospheric ELF/VLF oscillator. Different source characteristics related to simultaneous ground and satellite measurements have been also obtained in ref. [132].

Several successful experiments on ELF/VLF wave generation were carried out in Arecibo (Puerto Rico) where a powerful HF transmitter has modulated a current of the equatorial electrojet. In these experiments, the heater frequency and the radiated power were 3 MHz and ~800 kW, respectively, and the modulation frequencies were in the range from 500 to 5,000 Hz [133]. The efficiency of ionospheric ELF/VLF wave generator depending on the polarization of HF heater radiation and its daily work cycle was investigated by Ferrano in ref. [127].

High-frequency heating facility HIPAS located near Fairbanks (Alaska) was successfully used for the modulation of auroral electrojet in the experiment [134], in which the generation of ULF/ELF waves (11–76 Hz) with amplitudes ~1 pT at the phase modulation of a heater radiation has been observed. Villasenor et al. [135] have investigated the dependence of ELF/VLF wave generation efficiency on the modulation schemes of HF transmitter including the amplitude rectangular pulse modulation, phase and two frequency modulations. It was shown that the amplitude pulse modulation is most effective. ELF/VLF waves generated with the use of HIPAS heating facility have been observed in space plasma in ref. [136]. In this paper, in

contrast to similar measurements over the Tromso station [132], good correspondence between the satellite and ground-based measurements was demonstrated.

Experiments on generation of ELF/VLF waves with HAARP heating facility were carried out with use of different frequencies and polarizations of HF radiation [137]. It was shown that the possibility existed to control the polarization of artificially generated ELF waves by changing the frequency and the polarization of the heater radiation [137]. Within the framework of this Program the Stanford University has carried out a series of successful experiments on the injection of artificially excited ELF/VLF waves into the upper ionosphere and the Earth–ionosphere waveguide. Platino et al. [138] have reported the Demeter satellite observations of ELF/VLF emissions generated by HAARP heater in the ionosphere. For three of four modulation frequencies the satellite and the ground-based measurements have shown the same results corresponding to radiated power of ionospheric source ~3–4 W. Multi-hop magnetospheric echo of ELF/VLF signals induced by the HF transmitter have been observed by Inan et al. [3]. These echoes displayed dispersion and amplification in equatorial region of the magnetosphere leading to generation of trigger emissions. ELF/VLF waves excited by the HAARP heating facility were also injected into the Earth–ionosphere waveguide. Moore et al. [4] have demonstrated unique results of observations of HAARP-induced ELF emissions at the distance ~4,400 km from the heater. Characteristics of these emissions conformed to 4–32 W power of ionospheric oscillator at the altitude 75–80 km [4]. Long-term program of the experiments with HAARP HF transmitter performed by Stanford University have shown that heating of the lower ionosphere by powerful amplitude modulated HF radiation could be an effective tool for generation of ELF and VLF waves with given properties practically at any geomagnetic conditions [139].

The formation of VLF ducts (magnetic field-aligned channels of enhanced ionization) in the upper ionosphere recently detected by the Demeter satellite presents other important effect of the ionosphere HF heating. Characteristics of these ducts and other types of plasma disturbances and wave emissions observed over the heating facilities were presented in [6, 7, 140, 141]. Typical size of ducts across geomagnetic field was ~40 km at the satellite altitude and the plasma density excess within a duct over background level was 20–30%. Temperature and plasma density fluctuations in the ionosphere over the heating area were about 10–15%.

3.2.3 Influence of Powerful VLF Transmitters on the Ionosphere and the Magnetosphere

3.2.3.1 Artificially Stimulated Particle Precipitation into the Ionosphere

First experimental confirmation of artificial stimulation of radiation belt electron precipitation was obtained in 1975 by Zhulin et al. [142] with use of powerful

ground-based VLF transmitter located in Arkhangelsk region (Russia). Diagnostics of electron precipitation was performed by special optical devices installed onboard the aircraft-laboratory Yak-40. This experiment has shown significant enhancement in intensity of atmospheric emission at 557.7 nm correlated with periodic VLF transmitter pulses. Pulsations of the emission intensity were up to 40 R. An estimate of precipitating electron energy flux with account of the experiment's geometry has given $\sim$0.13 erg/cm^2·s (1.3×10^{-4} J/m^{2}s) that corresponded to flux of electrons with energy $\sim$15 keV approximately 5×10^4 particles/cm^2·s and was a factor of 10 above the background level.

Direct measurements of artificially stimulated electron precipitations from the radiation belt were carried out onboard the S81-1 satellite with use of USA VLF transmitters NAA and NSS [143–145] and independently by the Aureol-3 satellite [146, 147]. Bursts of precipitating electrons were observed by S81-1 satellite 1–2 s after commencement of the transmitter pulses [143, 144]. Similar delay followed from the theoretical estimates [145]. The most recent results on the electron precipitations stimulated by ground VLF transmitter were reported by Sauvaud et al. [148] and Gamble et al. [13], based on the Demeter satellite data.

3.2.3.2 Effects of the Ionosphere Heating by Powerful VLF Transmitters

Experiments on artificial stimulation of radiation belt electron precipitation led to discovery of the effect of lower ionosphere heating by the radiation from ground-based VLF transmitters with use of probe VLF signals [149]. First experiments were performed with NAU transmitter in Puerto Rico. About $\sim$100 kW power at 28.5 kHz were radiated by pulses of 3 s duration and 5 s repetition period. Search for lower ionosphere perturbations was carried out using probe signals from several US VLF transmitters at the receiving stations in Arecibo (Puerto Rico) and Palmer (the Antarctic). Data analysis revealed the 5 s periodicity in a spectrum of amplitude envelope of probe signals from the NAA transmitter. Perturbations of amplitude with the modulation period of heating transmitter were in the range from -0.04 to $+0.12$ dB [149]. It is interesting to note that such disturbances caused by 100 kW NAU VLF transmitter coincided in the order of magnitude with the heating effect of the Tromso HF transmitter, the effective radiated power of which was 200 MW [150]. This seeming contradiction was resolved by Taranenko et al. [151] who showed that the amplitude disturbances of probe VLF wave in the Earth–ionosphere waveguide in both cases should be comparable in magnitude since VLF heating is maximum at the reflection heights of subionospheric signals in *D*-region, and consequently the heating effect on the probe wave amplitude should be strongest there.

A series of purposeful experiments on VLF heating of the lower ionosphere was performed by Stanford University in the period from 1987 to 1992 [149]. In the experiment of 1992, the amplitude and phase perturbations of probe signals at 21.4 kHz from NSS transmitter in Annapolis (Maryland) were registered in Gander (Newfoundland). Investigated were the effects of ionosphere heating by the NAA

transmitter in Cutler (Maine) operating at 24 kHz. For monitoring measurements, the station in Gander received the NLK (24.8 kHz) and the NAU (28.5 kHz) signals whose great circle paths did not pass through the ionosphic region heated by the NAA transmitter. The ionosphere heating effect was found in 41 of 53 episodes of NAA transmitter "ON/OFF". The amplitude and phase perturbations of probe signals lie in the ranges from −0.11 to +0.84 dB and from 0 to −5.3°, respectively [152, 153]. In a similar experiment with the NLK transmitter as a heater, the observed perturbations of probe wave amplitude on the NPM (Hawaii) – Saskatoon (Saskatchewan) propagation path ranged from 0.3 to 1.6 dB [152, 153].

Strong ionospheric disturbances in the zone of powerful VLF transmitter NWC (Australia) were observed from the Demeter satellite [5]. Significant enhancement of electron temperature and fluctuations of electron and ion densities were recorded together with intensification of HF and ELF electrostatic waves. Dimension of the perturbation zone in the ionosphere at the satellite altitude (∼700 km) was about 800 km along the orbit, the position of center of this zone corresponded to L-shell of the NWC transmitter ($L = 1.41$).

Thus numerous experiments show that intense VLF waves from different sources influence on the lower ionosphere and therefore on the characteristics of radio wave propagation sensible to changes in the ionosphere parameters.

Three-dimensional (3D) theoretical modeling of the lower ionosphere heating by VLF transmitter radiation was carried out by Rodriguez and Inan [153] and Rodriguez [152]. The heated area in the ionosphere has a form of a spot with a radius of ∼150 km at the level half of the perturbation maximum. Position of maximum is slightly shifted to pole from the position of heater. For transmitters with radiated power ∼1,000 kW the electron temperature in maximum of heating (∼87 km) exceeds the undisturbed level approximately threefold.

3.2.3.3 Acceleration of Ionospheric Ions

Effect of acceleration of ions in the ionosphere under influence of radiation from ground-based VLF transmitter was first observed onboard the Aureol-3 satellite [8]. The observations were made in the zone of Arkhangelsk VLF transmitter (64° 24′N, 41° 32′E, $L = 4$), which radiated ∼300 kW power at the carrier frequency 19.1 kHz with amplitude modulation by periodic pulses (8 s ON–8 s OFF). The satellite instrumentation set provided measurements of ion distributions for $M = 1$–32 atomic mass units at energies from 0.01 to 3.5 keV/charge and pitch-angles 85° and 145° combined with analysis of electromagnetic fields in the frequency range from 10 Hz to 20 kHz.

The observations showed that a mid-latitude increase in H^+, He^+ and O^+ ion fluxes, of about an order of magnitude above the background level, at the energies 250–330 eV and pitch-angles 85° and 145° occurred in the zone, in which the transmitter signals were detected. Such quasi-transverse and upward ion fluxes with magnitude up to 10^6–10^7 $cm^{-2}{\cdot}s^{-1}{\cdot}sr^{-1}{\cdot}keV^{-1}$ were observed in five passages of the Aureol-3 satellite

over the zone of Arkhangelsk VLF transmitter. It is significant that the upward (145°) ion fluxes directed from the ionosphere into the magnetosphere were of the same order of magnitude as the quasi-transverse (85°) ion fluxes. Simultaneously with anomalous ions the VLF emission at the frequencies ~4.5 kHz well correlated with the transmitter pulses have been observed. These frequencies were close to local low hybrid resonance frequency. Let us note that the measurements were carried out in the conditions of low geomagnetic activity ($D_{st} = -10$), therefore the zone of natural auroral precipitations lied in higher latitudes.

From the discussed Aureol-3 data Dzhordzhio et al. [8] have concluded that intense electromagnetic waves radiated by ground VLF transmitter could stimulate acceleration up to 300 eV energy and injection into the magnetosphere of ionospheric O^+, He^+ , H^+ ions combined with excitation of ELF/VLF noises.

Due to high phase velocity of whistler mode waves, their interaction with supra thermal (<1 keV) ions in the ionosphere is not effective. For explanation of these experimental results, it seems reasonable to consider a two-step process – nonlinear conversion of whistler waves from the transmitter into other plasma modes and the subsequent interaction of these secondary waves with ionospheric ions. Mechanisms for transformation of waves and acceleration of ions are considered below.

Continuation of active experiments on the influence of VLF transmission on ion distributions and ELF/VLF emissions in the ionosphere has been performed by Chmyrev et al. [10]. These experiments were carried out onboard the COSMOS-1809 satellite using a Arkhangelsk VLF transmitter operated at frequencies 15 and 19.1 kHz in the same regime as above (300 kW radiated power, pulse modulation: 8 s ON–8 s OFF). The satellite was operating on the near circular orbit with altitude ~960 km and inclination 82.5°. Eight episodes of the transmitter operation were carried out during the satellite passages over the transmitter zone. Distance in longitude between the satellite trajectory and the transmitter location in these episodes was ≤30°.

Figure 3.1 shows the distribution of low-energy ion fluxes in the ionosphere over the transmitter zone obtained on the satellite orbit 1376, which was nearest to the transmitter. Each of the four panels in Fig. 3.2, which corresponds to different energy channels of electrostatic analyzer SF-3M, presents the ion fluxes for pitch-angles $\alpha = 5–40°$, 50–85°, 95–130°, 140–175°. In this episode, the transmission started at 20.30 UT when COSMOS-1809 crossed the L-shell of the transmitter ($L = 4$).

It is seen from Fig. 3.1 that effective heating of ions occurred in the ionosphere over the transmitter zone, where the flux of ions with energy 28–74 eV increased from the background level of 10^3 $cm^{-2}{\cdot}s^{-1}{\cdot}sr^{-1}{\cdot}keV^{-1}$ up to $(2–4){\cdot}10^4$ $cm^{-2}{\cdot}s^{-1}{\cdot}sr^{-1}{\cdot}keV^{-1}$ during the time smaller or of the order of 1 min. An important peculiarity of the particle distributions in Fig. 3.1 is that the downward ion fluxes were the strongest and the particles with higher energy appeared later (at higher L-shells). For precipitation and quasi-transverse fluxes, it means that particles accumulate energy at larger length or at higher altitudes along the line of magnetic field above the satellite. The characteristic transverse scale of the acceleration zone, as estimated from 28 eV ion distribution, is ~200 km at the satellite altitude ($h \approx 960$ km). The analysis

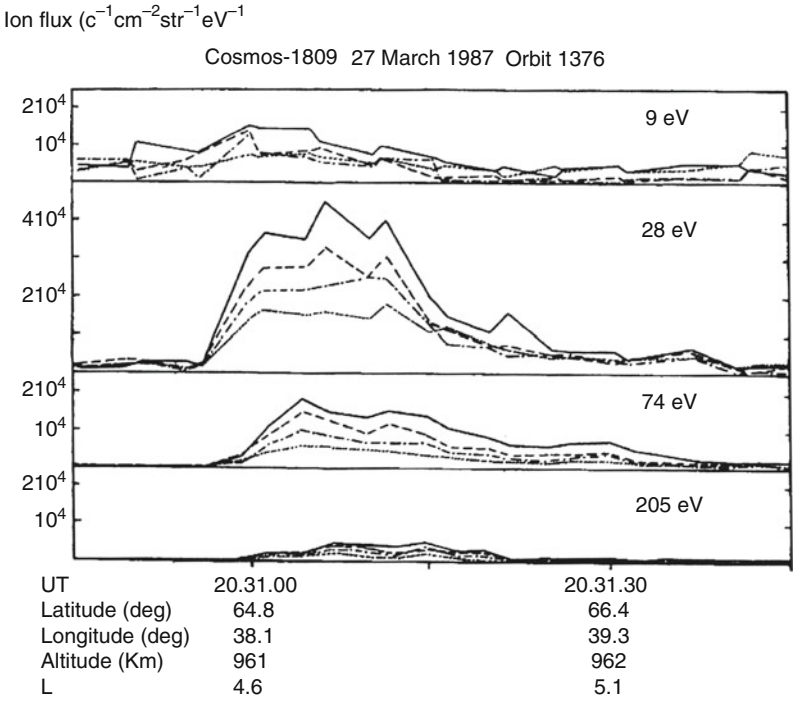

Fig. 3.1 Distribution of low energy ion fluxes along the orbit 1376 of COSMOS-1809 satellite over the Arkhangelsk VLF transmitter zone for energies ~ 9, 28, 74, and 205 eV and pitch-angles 5–40° (——), 50–85° (– – –) , 95–130° (– · –), and 140–175° (· · ·)

of energy spectrum of ions for all pitch-angles showed that the enhancement of ion fluxes in the transmitter zone took place in the range from 10 to 200 eV with maximum at 20–70 eV.

3.2.3.4 Parametric Excitation of ELF Waves in the Upper Ionosphere

Enhancement of intensity (stimulation) of ELF noises correlated with VLF transmissions was observed on three passages of COSMOS-1809 over the transmitter zone where the discussed above ion acceleration occurred [10]. Stimulated ELF emissions were found very near the transmitter (within $\pm 5°$ in longitudes and $\pm 3°$ in latitudes) in the region of maximum intensity of the transmitter signals. The spectral density of noises at the lower part ($f < 400$ Hz) of the device frequency range increased during the transmitter pulses 2–3 times above the undisturbed level observed in pauses between the pulses. A maximum of induced ELF wave intensity appeared to be at 140–180 Hz.

Spectra of VLF transmitter signals during the observation of stimulated ELF emissions at all three orbits was found to be broadened; the characteristic broadening was $\Delta f \sim \pm$ (200–400 Hz). This value corresponds to the frequency band of ELF emissions correlated with VLF transmitter pulses.

Let us note that the effect of spectral broadening of VLF signals in the ionosphere and the magnetosphere of the Earth were numerously observed from satellites and on the ground [154–157]. Titova et al. [156] interpreted this effect in terms of VLF signal scattering by low-frequency plasma turbulence (in particular the ion-cyclotron one) in the ionosphere below and/or near the satellite. At such scattering process the observed electrostatic ELF emissions were not correlated with the transmitter signals and the broadening effect took place for all transmitters independently on their power [156].

In the experiment [10] such scattering of VLF signals was also observed; ELF emissions in these cases were not correlated with transmitter pulses and the spectrum-broadening effect was registered for all VLF transmitters (independently on power) observed on satellite at the frequencies below 20 kHz. However, besides the scattering by ionospheric turbulence, the nonlinear VLF wave interaction process occurred in the experiment [10], which resulted in the generation of ELF waves and depended on the intensity of pump wave. Such conclusion was made based on the correlation between the observed ELF emissions and the transmitter signals and also from the fact that spectrum broadening in such events has been observed only for powerful signals. The latter followed from the comparison of simultaneously observed signals of the Arkhangelsk VLF transmitter (radiated power ~300 kW) at 19.1 kHz with signals from the OMEGA transmitter in Norway (radiated power ~10 kW) at 10.2 kHz.

The measurements of wave intensity in separate spectral channels showed that the propagation of a strong electromagnetic wave from a VLF transmitter through the ionosphere was accompanied by the generation of rather intense (~8 $\mu V/m \cdot Hz^{1/2}$) secondary emissions in the electric field at frequencies ~140 Hz. This emission was well correlated with the transmitter signals, while other spectral channels did not indicate any reaction on the transmitter operation. However, magnetic component of the emission at 140 Hz did not exceed the level of noise (~0.3 $pT/Hz^{1/2}$). The filter bandwidth in a channel 140 Hz of the spectrum analyzer was ~20 Hz. The ratio of magnetic-to-electric field components for the transmitter signals was $N = B/E \approx 18$ that corresponded to the refraction index of the whistler mode wave.

Thus, the presented experimental results confirm the generation of ELF waves and acceleration of ionospheric ions under the influence of strong VLF transmissions. Before considering physical mechanisms for such influence, let us resume the main characteristics of the observed phenomena:

- The excitation of ELF emissions correlating with Arkhangelsk VLF transmitter signals was observed in the frequency range 70–400 Hz with maximum intensity ~8 $\mu V/m \cdot Hz^{1/2}$ at frequencies 140–180 Hz.
- Simultaneously, with the generation of ELF emissions, the spectral broadening $\Delta f = \pm$ (200–400 Hz) was observed in Arkhangelsk transmitter signals while

broadening of weaker signals from the OMEGA transmitter in the same zone was not found.

- The enhancement of ion flux in the transmitter zone took place in the range of energies from 10 to 200 eV; maximum of flux intensity $\sim(2–4)\cdot10^4$ $cm^{-2}\cdot s^{-1}\cdot sr^{-1}\cdot eV^{-1}$ was observed at 20–70 eV.
- Accelerated ion fluxes were anisotropic; the highest anisotropy was observed at ~28 eV.

As we mentioned the interaction of low energy ($\leq$1 keV) ions with whistler waves at the transmitter frequencies and in ELF range is not effective due to high phase velocities of these waves in the ionosphere. Therefore, it was reasonable to suppose that suprathermal ions were accelerated by one of the ion branches of plasma waves, which could be excited due to parametric instability of intense whistler mode waves. In the frequency range 70–400 Hz, it could be electrostatic ion-cyclotron waves, ion-acoustic, and electromagnetic ion-cyclotron waves, the generation of which has been considered in many papers (see, e.g. [158, 159]). The highest growth rates are realized in a process of decay interaction of whistler with low frequency plasma wave and ion-cyclotron wave. Detailed analysis of the ion wave modes generation by decay instability of quasimonochromatic whistler waves with account of several types of ions and variations of ion composition with altitude in the ionosphere has been performed by Chmyrev et al. [160]. Effectiveness of decay process with participation of electromagnetic ion-cyclotron waves in the ionosphere is substantially higher than with electrostatic waves due to strong linear attenuation of latter [159]. Electromagnetic ion-cyclotron waves present one of the most effective sources of ion acceleration in the upper ionosphere [161]. With account of these circumstances Taranenko and Chmyrev [159] and Chmyrev et al. [160] suggested the following scheme for explanation of the above-discussed experimental results. Intense whistler mode wave from the ground VLF transmitter decays in the upper ionosphere on other whistler propagating near the resonance cone and highly oblique left-polarized electromagnetic ion-cyclotron wave. The ion waves propagating upward in the region of decreasing geomagnetic field will be effectively absorbed by ions providing their acceleration. This mechanism is similar to [161] with the difference that in [161] the electromagnetic ion-cyclotron waves are excited due to instability of precipitating auroral electrons while in [159, 160] – due to parametric instability of intense whistler waves. Analysis of growth rates γ_1 and frequencies ω_3 of electromagnetic ion-cyclotron waves for this process showed that excitation was possible only for waves with large transverse components of wave vectors [159]. The corresponding frequency range $\omega_3 \approx$ 100–350 Hz calculated for altitudes below 2,000 km was in agreement with the data on generation of ELF emissions and VLF wave spectra broadening. Maximum growth rate was $\gamma_1 \approx$ 2–3 s^{-1} at the amplitude of pump wave ~10 mV/m [159].

Let us consider now the interaction of parametrically excited electromagnetic ion-cyclotron waves with ions [10]. Dispersion equation for these waves as known can be written as follows:

$$\omega_3 = k_{||3} v_A (1 - {\omega_3}^2/{\omega_{Bi}}^2)(1 + \kappa^2)^{-1/2}, \ \kappa = ck_{\perp 3}/\omega_{pe}, \tag{3.1}$$

where $k_{\|3}$, $k_{\perp 3}$ are longitudinal and transverse components of wave vector, ω_{Bi} is cyclotron frequency of ions, v_{A} is Alfven velocity, c and ω_{pe} are light velocity and electron plasma frequency. Resonance energy of ions interacting with wave (3.1) at first cyclotron resonance is defined as

$$W_{//\mathrm{res}} = \frac{Mv_{//\mathrm{res}}^2}{2} = \frac{Mv_{\mathrm{A}}^2}{2}\left(1 - \frac{\omega_3^2}{\omega_{\mathrm{Bi}}^2}\right)\left(\frac{\omega_{Bi}}{\omega_3} - 1\right)^2 (1+\kappa^2)^{-1}, \tag{3.2}$$

where $v_{//\mathrm{res}} = (\omega_{\mathrm{Bi}} - \omega_3)/k_{//3}$, M is ion mass, $v_{//\mathrm{res}}$ and $k_{//3}$ are oppositely directed. Let us estimate $W_{//\mathrm{res}}$ for H^+ ions in the ionosphere at altitudes ~2,000 km, where $v_{\mathrm{A}} \approx 10^8$ cm/s. At $\kappa = 3$, which corresponds to maximum growth rate we find $W_{//\mathrm{res}} = 1.3$ eV for frequency $\omega_3/\omega_{\mathrm{Bi}} = 0.9$ and $W_{//\mathrm{res}} = 12.5$eV for frequency $\omega_3/\omega_{\mathrm{Bi}} = 0.8$.

Following ref. [161], let us estimate an effectiveness of resonance heating of ions in the conditions of the above-considered experiment [10]. We assume that some part of the geomagnetic field tube is filled by electromagnetic ion-cyclotron waves, born in the decay process, with a sufficient wide-frequency band so that in every part of the trajectory in an inhomogeneous magnetic field, the particle could find the wave, which satisfies the condition of local cyclotron resonance and therefore experiences continuous acceleration along the trajectory. The transverse energy increment of resonance ion can be written as

$$\Delta W_{\perp} = \frac{M(\Delta V_{\perp})^2}{2} = \frac{e^2 E_{\perp 3}^2}{2M}(\Delta t)^2,$$

where e and M are particle charge and mass, $E_{\perp 3}$ is transverse component of wave electric field, Δt is a time of particle being in resonance with wave. In the vicinity of resonance frequency, one may assume ${E_{\perp 3}}^2 = P(f)\Delta f$, where $P(f)$ is a spectral density of the emission and Δf is the frequency bandwidth. For the wide band wave packet, it is possible to believe the resonance time Δt to be equal to the characteristic time of phase correlation in the packet, that is, $\Delta t \sim (\Delta f)^{-1}$. Then, for the energy growth rate, we obtain [161]

$$\frac{\mathrm{d}W_{\perp}}{\mathrm{d}t} == \frac{e^2 P(f)}{2M}. \tag{3.3}$$

The movement of a particle in an inhomogeneous magnetic field $B_0(s)$ in approximation of a leading center with an account of Eq. (3.3), neglecting the geomagnetic field-aligned electric field, is described by the following equations [161]:

$$\frac{\mathrm{d}W_{\perp}}{\mathrm{d}t} = W_{\perp} v_{//} B_0^{-1} \mathrm{d}B_0/\mathrm{d}s + e^2 P(f,s)/2M, M\frac{\mathrm{d}v_{//}}{\mathrm{d}t} = -W_{\perp} B_0^{-1} \mathrm{d}B_0/\mathrm{d}s, \tag{3.4}$$

where $v_{//}$ is longitudinal velocity of particle, $W_{\perp}$ is transverse energy, and ds is an element of length. For dipole magnetic field, Eq. (3.4) has a form

$$v_{//}\frac{2dW_{\perp}}{2d\varphi} = v_{//}W_{\perp}\frac{3\ \sin\varphi(3+5\ \sin^2\varphi)}{\cos\varphi(1+3\ \sin^2\varphi)} + \frac{e^2P(f,\varphi)}{2M}LR_0\cos\varphi(1+3\ \sin^2\varphi)^{1/2},$$

$$Mv_{//}\frac{2dv_{//}}{2d\varphi} = -W_{\perp}\frac{3\ \sin\varphi(3+5\ \sin^2\varphi)}{\cos\varphi(1+3\ \sin^2\varphi)} \tag{3.5}$$

where φ is geomagnetic latitude, L is McIlwain parameter, and R_0 is the Earth's radius. When obtaining Eq. (3.5) we assumed $\mathrm{d}/\mathrm{d}t = v_{//}(\partial\varphi/\partial s)\mathrm{d}/\mathrm{d}\varphi$.

Numerical integration of Eq. (3.5) along the part of magnetic field line at $L = 4.64$, where ion acceleration took place was performed in [10]. Integration was carried out in the range of $\Delta\varphi$ from initial latitude φ_0 corresponding to altitude h at a given magnetic field line downward to final latitude $\varphi_1 = 61.3°$ corresponding to altitude 450 km. While calculating, it was assumed that electromagnetic ion-cyclotron waves were generated along a geomagnetic field line and that their intensity was constant ($\mathrm{d}P/\mathrm{d}\varphi = 0$) within $\Delta\varphi$. A resonant particle with initial parallel energy $W_{//0}$ in the point $\varphi = \varphi_o$ was moving downward. Calculations were made for H^+ ions with initial transverse energy $W_{\perp 0} = 0$ and initial parallel energies $W_{//0} = 12.5$ and 6.25 eV. Spectral density of electromagnetic ion-cyclotron waves was taken according to experimentally observed value $P = 8 \times 10^{-11}\ \mathrm{V^2\ m^{-2}Hz^{-1}}$. It was found that at this wave intensity, the particle energy increase could reach $\Delta W \approx 20$–30 eV in the interval $\Delta\varphi = 3$–$5°$, which corresponds to interval of heights $\Delta h \approx 1{,}400$–$2{,}300$ km on a given magnetic field line. Pitch-angle, with which the particle comes to satellite at the altitude ~1,000 km, depends on the altitude (or latitude $\Delta\varphi$) and on initial parallel energy, from which this particle starts acceleration. The particles accelerated at altitudes below satellite and the accelerated particles came from above and turned back in mirror points below 1,000 km provide some upward flux corresponding to pitch-angles $\alpha > \pi/2$. All these characteristics are in agreement with the experiments.

So this modeling shows that the mechanism of ion acceleration by electromagnetic ion-cyclotron waves generated by parametric instability of strong VLF waves in the ionosphere is sufficiently effective to explain existing experimental data.

The VLF transmitter described in ref. [8] started to work several hours before satellite arrival in the transmitter zone, and there was enough time for pumping the accelerated particles into the wide range of geomagnetic field tubes (life time of such accelerated particles is $\sim 10^4$ s). Experimental data from COSMOS-1809 collected at orbit 1376 allow to analyze the development of ion acceleration process in time and in altitudes along geomagnetic field lines since the transmitter located at $L = 4$ was switched on at 20.30 UT, when the satellite was practically on the same L-shell ($L = 3.9$). Thus, the accelerated ions whose velocities exceed the velocity of satellite could reach the satellite only at higher L-shells moving to it from the acceleration region, while the magnetic field tube is not completely filled by

accelerated particles. Note that the lower energy (10–200 eV) accelerated ions measured by COSMOS-1809 could be observed in a wider range of latitudes than 250–330 eV analyzed in ref. [8]. On the whole, the presented results of ion measurements onboard the COSMOS-1809 satellite do not contradict the AUREOL-3 observations [8].

Though the scientific instruments onboard the COSMOS – 1809 did not analyze mass distribution of ions, we can assume that anomalous ion fluxes observed at orbit 1376 have been accelerated in the upper ionosphere at altitudes below several thousand kilometers. At the same effectiveness and location of acceleration mechanism, the O^+ ion needs by a factor of 4 longer time to reach the satellite altitude than the H^+ ion. With account of the discussed data this means that the oxygen ions could be observed by satellite only from narrower range of altitudes near the satellite trajectory (or significantly later when satellite was far away from the transmitter). Moving downward from the acceleration region at the sufficient parallel velocity the H^+ ions started at several thousand kilometers and the O^+ ions from the lower altitudes could be able to "run down" the satellite on ascending orbit at $L > L_{\Pi}$, where L_{Π} is the transmitter L-shell.

So the presented materials can be considered as experimental evidence of the acceleration processes in the upper ionosphere initiated by electromagnetic radiation from the powerful VLF transmitter. As a confirmation of this thesis, we can mention the observation of 630 nm [OI] and H_β atmospheric emissions from the "Intercosmos-Bulgaria 1300" satellite, which demonstrated the possibility of stimulation (or intensification) of these emissions due to forming the fluxes of accelerated ions and suprathermal electrons under the influence of intense VLF waves [9].

3.2.3.5 Artificial Stimulation of Geomagnetic Pulsations

In 1975 Frazer-Smith and Cole from Stanford University first paid attention on the fact that powerful ground-based VLF transmitters influenced on the generation regime of geomagnetic pulsations [162]. They have shown that the occurrence rate and the intensity of Pc-1 oscillations increased when the VLF transmitter located near the registration site operated.

Beginning from 1975 the Institute of Terrestrial Magnetism, Ionosphere and Radio Wave Propagation of Russian Academy of Sciences (IZMIRAN) has carried out a series of active experiments on the ionosphere modification by electromagnetic radiation from VLF transmitters. Below we consider the results of these experiments related to artificial stimulation of geomagnetic pulsations.

First of these experiments called "Juliana" has been carried out in February 1975 with use of Arkhangelsk VLF transmitter operated for this experiment at the frequency 12.5 kHz in the mode of amplitude pulse modulation, 15 s ON–15 s OFF. Module magnetic measurements were carried out at IZMIRAN expedition base ~200 km away from the transmitter. Data reduction of the magnetic records with use of the epoch superposition method revealed an excitation of the magnetic field oscillations with the repetition period (30 s) of the transmitter signals and with amplitude ~16 nT

[163]. In pauses between the transmissions, no regular 30 s oscillations were observed. This observation was the first direct experimental evidence of artificial generation of geomagnetic pulsations under influence of VLF transmitter on the ionosphere and the magnetosphere.

The experiments of 1987 were also carried out with use of Arkhangelsk VLF transmitter. The radiated power was 300 kW, the carrier frequencies were 15 and 19.1 kHz, and the modulation regimes were 2 s ON–2 s OFF, 8 s ON–8 s OFF, and 50 s ON–10 s OFF. Measurements of geomagnetic pulsations were performed at Lekhta station in Karelia (Russia) and at Oulu, Kevo, and Sodankyla stations in Finland. In these experiments the ground-based geomagnetic observations were accompanied by the measurements of ELF/VLF waves and particle fluxes onboard the COSMOS-1809 satellite.

Figure 3.2 shows one of the episodes of artificial stimulation of geomagnetic oscillations [164]. In this episode the transmitter was operating in the modulation regime 8/8 during the night time in quiet geomagnetic conditions. Presented are the wave forms of *D*-component of geomagnetic pulsations recorded in Lekhta in two frequency channels (LF: 0.005–1.0 Hz and HF: 0.1–1.0 Hz) and the spectrogram of *H*-component of geomagnetic pulsations observed in Kevo. The bar near 21.00 UT in the lower part of Fig. 3.2 indicates the time interval when transmitter was active.

It is seen from Fig. 3.2 that the pulsation bursts of *Pi*-1 and *Pi*-2 types have appeared 10–15 min after beginning of transmitter operation and terminated approximately 15 min after transmitter switching off. Maximum amplitudes were ~0.1 nT (HF channel) and ~4 nT (LF channel) [164].

We already discussed the COSMOS-1809 satellite data on 9–205 eV ions observed over the transmitter zone during this episode (see Fig. 3.1). When the ground

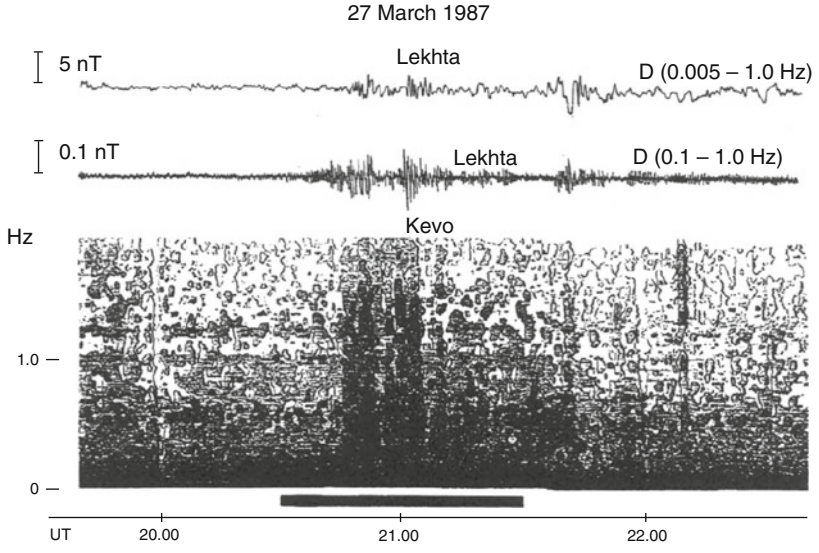

Fig. 3.2 Wave forms of the magnetic field oscillations (*D* – component) at Lekhta station and the spectrogram of geomagnetic oscillations (*H* – component) observed at Kevo station 27 March 1987

multistation measurements indicated the generation of geomagnetic oscillations, the satellite observed significant enhancement of ion fluxes with energies 9–205 eV in narrow zone $\leq 3^\circ$ above transmitter, the maximum $\sim 4 \times 10^4$ cm^{-2}s^{-1}sr^{-1}eV^{-1} was at 20–70 eV [10]. This combination of simultaneous ground and satellite observations has given a base for assumption that the generation of *Pi*-1 and *Pi*-2 geomagnetic pulsations in this case was stimulated by the VLF transmitter [164].

The characteristic time delay between the commencement of VLF transmission and the appearance of stimulated magnetic oscillations was about 10–15 min. Owing to such conjunction in observations of geomagnetic pulsations and accelerated ions it was natural to conclude that transmitter influence on the generation of magnetic oscillations was performed by means of artificially accelerated ionospheric ions carried into the magnetosphere.

VLF transmitter-induced formation of conic ion distributions and transfer of accelerated ionospheric ions (O^+, He^+, and H^+) into the magnetosphere was observed from the AUREOL-3 satellite [8] as we already discussed.

The considered experimental data have been used for the development of theoretical model of artificially stimulated geomagnetic oscillations [160, 164]. According to this model transverse acceleration of ions takes place in the upper ionosphere below 2,000 km, where the intensities of injected VLF waves and of parametrically excited ELF emissions are sufficiently high, while the generation (amplification) of geomagnetic oscillations by accelerated ions occurs in the magnetosphere (mainly in the near equator region), where the magnetic field and plasma spatial gradients are small. The time delay between the commencement of VLF wave injection and the appearance of geomagnetic pulsations is about the time needed for accelerated ions to fill up the magnetic field tube in the acceleration zone. The estimates made in refs. [160, 164] have shown that the ion fluxes observed in the discussed experiments could provide the amplification of oblique Alfven waves in the magnetosphere near $L \approx 4$ with exponential growth rate ~ 0.2 s^{-1} for frequencies ~ 5 Hz and ~ 0.05 s^{-1} for frequencies ~ 0.5 Hz. At such growth rates the stimulation of geomagnetic pulsations could be provided at the time scale of the order of several minutes.

3.3 Electric Current and Field Perturbation in the Atmosphere–Ionosphere Circuit

3.3.1 Equations Describing the Electric Potential in the Ionosphere

The below-considered electrodynamic model of electromagnetic and plasma precursors to earthquake was formulated in refs. [21, 165] to explain some of the observed phenomena by the electric field enhancement in the ionosphere over a seismically active zone. The idea of such explanations arose from the observations

of anomalous DC electric fields ~10 mV/m in the low-latitude ionosphere over a region shortly before an earthquake [45]. An existence of seismic-related electric fields and their possible role in the lithosphere–ionosphere coupling were discussed in refs. [38, 43, 166, 167]. The main conclusion made in these papers was that to excite more or less significant (≥1 mV/m) electric field in the ionosphere, the vertical component of long-term DC electric field on the Earth's surface should be ~1–10 kV/m in the area ~100 km. Such fields at the time scale about several days have never been observed. Vershinin et al. [42] reported the observation of short-time (1–2 h) bursts of the localized vertical electric field ~500 V/m 8–10 h before an earthquake. According to Buchachenko et al. [15], the meaningful ionospheric precursors should exist at least for several days. The long-time electric field variations observed before earthquakes have a magnitude ~100 V/m or less [42]. So for proper modelling, we should find the mechanism providing the generation of ~10 mV/m electric field in the ionosphere at slow variations of the vertical electric field near the Earth's surface with magnitude ~100 V/m or below.

Such mechanism based on the electric field perturbation by the conductivity currents in the atmosphere and the ionosphere was suggested in refs. [30, 168]. Their source was an external electric current generated by the injection of charged aerosols into the atmosphere with soil gases, the upward transfer of these aerosols, and their gravitational sedimentation with charge relaxation. Evidently the time scales of the external current generation and the injection of soil gases into the atmosphere should be similar.

Let us consider the generation of the electric field perturbation by an external current $\mathbf{j_e}$ in the Earth–ionosphere layer. We will find a system of equations that determine the potential φ of the electric field perturbation $\mathbf{E} = -\nabla \cdot \varphi$. Let us introduce Cartesian coordinates $(x, y, z)$with the z-axis directed vertically upward. The homogeneous magnetic field $\mathbf{B}$ is directed at epy angle of α with respect to the x-axis. The $z = 0$ plane coincides with the ideally conducting Earth's surface. We assume that the electric field potential is zero on this plane, $\phi|_{z=0} = 0$. The layer $0 < z < z_1$ is the atmosphere, whose conductivity $\sigma(z)$ depends on the altitude z. The $z = z_1$ plane coincides with the thin conducting ionosphere characterized by the integral conductivity tensor with the components Σ_P, Σ_H (the Pedersen and Hall conductivities, respectively). According to refs. [30, 168], for slow processes with characteristic times $t \gg 1/\sigma$, the distribution of the horizontal electric field components in the ionosphere is derived by the equations:

$$
\begin{aligned}
E_x(x,y) &= \frac{1}{4\pi\Sigma_P} \int_{-\infty}^{\infty} \int_{-\infty}^{\infty} K_x(x-x', y-y')\, j_1(x', y')\, \mathrm{d}x'\, \mathrm{d}y';\\
E_y(x,y) &= \frac{1}{4\pi\Sigma_P} \int_{-\infty}^{\infty} \int_{-\infty}^{\infty} K_y(x-x', y-y')\, j_1(x', y')\, \mathrm{d}x'\, \mathrm{d}y';\\
K_x(x,y) &= \frac{x \sin^3 \alpha}{x^2 \sin^2 \alpha + y^2}; \quad K_y(x,y) = \frac{y \sin \alpha}{x^2 \sin^2 \alpha + y^2}.
\end{aligned}
\tag{3.6}
$$

Equations (3.6) are used to calculate the spatial electric field distribution in the ionosphere.

3.3.2 Electric Field Limitation on the Earth's Surface

As mentioned above, the long-time (∼ several days) variations of the electric field on the ground do not exceed ∼100 V/m. Such limitation can be connected with the feedback between the vertical electric field perturbation and the causative external electric current near the Earth's surface [30]. The feedback is provided by the potential barrier at the Earth–atmosphere boundary that controls the upward moving of charged aerosol particles through this boundary. The movement occurs owing to viscosity of soil gases injected into the atmosphere. For instance, if a positively charged particle emerges from the Earth into the atmosphere, the Earth's surface gets charged negatively, and the electric field that appears, which is directed downward, impedes particle emergence to the surface. At the same time, this field stimulates the emergence of negatively charged particles onto the surface.

The vertical electric field component in the atmosphere $E_z = -\partial\varphi/\partial z$ is defined by the following equation [30]:

$$E_z(\mathbf{r},z) = \frac{1}{\sigma(z)}\left[j_1(\mathbf{r}) - j_e(\mathbf{r},z)\right]; \quad j_1(\mathbf{r}) = \int_0^{z_1} \frac{j_e(\mathbf{r},z)}{\sigma(z)}\mathrm{d}z \Big/ \int_0^{z_1} \frac{\mathrm{d}z}{\sigma(z)}. \tag{3.7}$$

We assume that an external current is formed as a result of the injection of positively (j_p) and negatively (j_n) charged soil aerosols into the atmosphere,

$$j_e(x,y,z) = j_p(x,y)s_p(z) - j_n(x,y)s_n(z); \quad s_p(z=0) = s_n(z=0) = 1.$$

The $s_p(z)$ and $s_n(z)$ functions describe the altitude distribution of external currents. Substituting the above equality into Eq. (3.7) yields an equation for the vertical electric field component on the Earth's surface, namely,

$$\begin{aligned} E_{z0}(x,y) &= \frac{1}{\sigma_0}\left[j_1(x,y) - j_p(x,y) + j_n(x,y)\right]; \\ j_1(x,y) &= \frac{1}{\rho}\left[j_p(x,y)k_p - j_n(x,y)k_n\right]. \\ E_{z0}(x,y) &= E_z(x,y,z=0); \quad \sigma_0 = \sigma(z=0); \\ k_{p,n} &= \int_0^{z_1} \mathrm{d}z \frac{s_{p,n}(z)}{\sigma(z)}; \quad \rho = \int_0^{z_1} \frac{\mathrm{d}z}{\sigma(z)} \end{aligned} \tag{3.8}$$

External currents of positively and negatively charged aerosols depend on the vertical electric field component on the Earth's surface as required by the feedback mechanism,

$$j_{\mathrm{p}}(x,y) = j_{\mathrm{p0}}(x,y) f\left(E_{z0}(x,y)/E_{\mathrm{cp}}\right); \quad j_{\mathrm{n}}(x,y) = j_{\mathrm{n0}}(x,y) f(-E_{z0}(x,y)/E_{\mathrm{cn}}),$$

where $j_{\mathrm{p0}}(x,y)$, $j_{\mathrm{n0}}(x,y)$ are determined by the intensity of charged aerosols injection in the absence of an electric field. When the negative field reaches some critical value E_{cp}, it blocks the flow of positively charged particles. Accordingly, a positive field blocks the flow of negatively charged particles. The critical field can be estimated in the order of magnitude from the balance equation for viscous, gravity, and electrostatic forces,

$$E_{\mathrm{cp}} = (6\ \pi\eta R_{\mathrm{p}} V - m_{\mathrm{p}} g)/eZ_{\mathrm{p}}; \quad E_{\mathrm{cn}} = (6\ \pi\eta R_{\mathrm{n}} V - m_{\mathrm{n}} g)/eZ_{\mathrm{n}},$$

where η is the viscosity of air, V is the velocity of upward movement of soil gases in earth, $R_{\mathrm{p,n}}$ is the aerosol particle radius, $m_{\mathrm{p,n}} = (4/3)\ \pi R_{\mathrm{p,n}}^3 \mu$ is the particle mass, and μ is the particle density. The viscous force of soil gases that rise in the Earth acts on a particle upward. The gravity force is directed downward. The electrostatic force, which appears as a result of the emergence of a positively charged particle onto the surface, is directed downward. For simplicity, we assume that positively and negatively charged aerosols have equal sizes and masses, $E_{\mathrm{cp}} = E_{\mathrm{cn}} = E_{\mathrm{c}}$. To perform calculations, let us specify the functional dependence f on the electric field as $f = \sqrt{1 + E_{z0}/E_{\mathrm{c}}}$. Using this dependence in Eq. (3.8) yields

$$E_{z0}(x,y) = \frac{1}{\sigma_0}\left[j_{\mathrm{p0}}(x,y)\left(\frac{k_{\mathrm{p}}}{\rho} - 1\right)\sqrt{1 + \frac{E_{z0}(x,y)}{E_{\mathrm{c}}}} - j_{\mathrm{n0}}(x,y)\left(\frac{k_{\mathrm{n}}}{\rho} - 1\right)\sqrt{1 - \frac{E_{z0}(x,y)}{E_{\mathrm{c}}}}\right]. \tag{3.9}$$

Given j_{p0}, j_{n0}, this equation allows us to calculate the vertical electric field component on the Earth's surface. After solving Eq. (3.9), we can determine the horizontal distribution of the conductivity current flowing from the atmosphere into the ionosphere. It follows from Eqs. (3.8) and (3.9) that

$$j_1(x,y) = \frac{1}{\rho}\left[j_{\mathrm{p0}}(x,y)\sqrt{1 + \frac{E_{z0}(x,y)}{E_{\mathrm{c}}}}k_{\mathrm{p}} - j_{\mathrm{n0}}(x,y)\sqrt{1 - \frac{E_{z0}(x,y)}{E_{\mathrm{c}}}}k_{\mathrm{n}}\right]. \tag{3.10}$$

Let us assume $\eta = 1.72 \times 10^{-7}$ kg/(cm·s), $V = 10^{-4}$ m/s, $R = 5 \times 10^{-7}$ m, $\mu = 1.5 \times 10^3$ kg/m^3, and $Z = 100$. Then the estimates of the critical field give $E_{\mathrm{c}} = 450$ V/m and $\sigma_0 E_{\mathrm{c}} = 10$ pA/m^2. It means that the vertical electric field on the Earth's surface cannot exceed the value $E_{\mathrm{zm}} = 90$ V/m.

3.3.3 Mechanisms of External Electric Current Generation in the Lower Atmosphere

Various mechanisms can be responsible for the formation of external currents in the near-ground atmospheric layer [169, 170]. One of the most effective mechanisms is associated with intensification of charged soil aerosol injection into the atmosphere or with changes in meteorological conditions at a stable altitude distribution of aerosols. It was experimentally shown [23–27] that, several days before an earthquake, the concentration of metal ion-containing soil aerosols in the atmosphere increases by one or two orders of magnitude. The quasi-stationary aerosol distribution is formed as a result of turbulent upward transfer and gravitational sedimentation. Turbulent transfer occurs due to two main reasons. First is connected with vertical gradient of horizontal wind velocity and transformation of wind kinetic energy into the energy of turbulent pulsations. Second is caused by the thermal instability of the atmosphere arising when negative temperature gradient exceeds its adiabatic gradient. Turbulent vortices transfer aerosols from the altitudes, where their concentration N is high to the altitudes of a lower concentration. Equilibrium is attained when the vertical flux of aerosols is balanced by their gravitational sedimentation at the rate w.

For describing the dynamics of particles determined by stochastic differential equations we will use the probability distribution function $f(q,z,t)$ of aerosols, which has the meaning of a probability that a particle has the charge q at the time t and the altitude z [21]. If transport coefficient K weakly depends on the altitude, the kinetic equation for the $f(q,z,t)$ distribution function takes the form [21]:

$$\frac{\partial f}{\partial t} - w\frac{\partial f}{\partial z} - 4\ \pi\sigma(z)\frac{\partial}{\partial q}(qf) = K\frac{\partial^2 f}{\partial z^2}.$$

The space–time distributions of aerosol concentration, $N(z,t)$, their electric charge density, $\rho_e(z,t)$, and the density of external current connected with their motion, $j_e(z,t)$, can be written in terms of the moments of the $f(q,z,t)$ distribution function. The equation for the moments has a form

$$\frac{\partial N}{\partial t} - w\frac{\partial N}{\partial z} = K\frac{\partial^2 N}{\partial z^2};\quad \frac{\partial \rho_e}{\partial t} + 4\ \pi\sigma(z)\rho_e = -\frac{\partial j_e}{\partial z}.$$

The last equality describes the density of external charge and current in a conducting medium. Changes in the number of external charges in a distinguished volume are determined by two processes. First, this is electromotive force-induced transfer through the surface that bounds this volume. Secondly, there is a decrease in the external charge caused by its relaxation in the environment with conductivity σ. For instance, if the total flux of external charges through the surface binding the volume becomes zero $\nabla \cdot \mathbf{j}_e = 0$, the number of these charges in the volume decreases according to the law $\rho_e \sim \exp(-4\pi\sigma t)$. The relaxation time is $\sim 1/4\pi\sigma$.

If the process is fairly fast ($t \ll 1/4\pi\sigma$), charges fail to relax, and the continuity condition takes the form $\partial\rho_e/\partial t + \nabla \cdot \mathbf{j}_e = 0$. Otherwise, if external charges are formed at a low rate ($t \gg 1/4\pi\sigma$), the external charge density is connected with the external current as $4\pi\sigma\rho_e + \nabla \cdot \mathbf{j}_e = 0$. This equality means that, in the stationary state, the disappearance of external charges in the volume due to relaxation is balanced by their transfer through the boundary surface. We assume that the characteristic time of the processes under consideration is longer than the relaxation time $1/4\ \pi\sigma$. Equation for the altitude distribution of external current in the quasi-stationary approximation can be found from the above consideration in the following form:

$$\frac{\partial}{\partial z}\left[\frac{1}{4\pi\sigma(z)}\frac{\partial j_e(z,t)}{\partial z}\right] + \frac{w}{4\pi\sigma(z)K}\frac{\partial j_e(z,t)}{\partial z} - \frac{j_e(z,t)}{K} = 0.$$

An influence of variations in conductivity and radioactivity in the lower atmosphere on DC electric field over a seismic region was investigated by Sorokin et al. [171]. This effect is associated with the occurrence of ionization source due to seismic-related emanation of radon and other radioactive elements into the atmosphere. The natural radioactivity of the lower atmosphere is mainly associated with such elements as radon, radium, thorium, actinium, and their decay products. Radioactive elements enter the atmosphere together with soil gas, and then they are transferred by the air streams upwards up to the altitude of a few kilometers. An increase in the level of atmospheric radioactivity, for example, prior to an earthquake, leads to an increase in the ion production rate q. The number density of light ions and the mean charge of aerosols are determined by recombination of ions and their adhesion to aerosols at given ionization sources. The vertical distribution of ion production rate is formed as a result of atmospheric absorption of gamma radiation and alpha particles from the decay of radioactive elements in the atmosphere. The total ion production rate in the lower atmosphere is formed by two sources – the cosmic rays and the atmospheric radioactivity. To calculate the external current and the atmosphere conductivity, it is necessary to find an equilibrium ion number density depending on the ion formation rate. The equilibrium value of ion number density is defined by their recombination in the air and adhesion to aerosols. The perturbations of conductivity and external electric current as a function of altitude have been calculated from the following equations [171]:

$$H_{p,n}\frac{d}{dz}\left(\frac{1}{\sigma}\frac{dj_{p,n}}{dz}\right) + \frac{1}{\sigma}\frac{dj_{p,n}}{dz} - \frac{j_{p,n}}{2\varepsilon_0 v_{p,n}} = 0; \quad \sigma = 2e\mu n,$$

$$n = \sqrt{N^2 + n_0^2} - N; \quad N = \frac{e\mu}{4\varepsilon_0\alpha}\left(\frac{N_p}{\lambda_p} + \frac{N_n}{\lambda_n}\right); \quad n_0 = \sqrt{\frac{q}{\alpha}}$$

where $\sigma = 2e\mu n$ is the atmospheric conductivity, n_0 is the ion number density in the clean atmosphere without aerosols, $N_{p,n}$ are the positive and negative aerosol number densities, α is the recombination constant, and μ is the light ion mobility in the atmosphere. Rapid growth of the conductivity occurs in the near surface layer.

At altitudes up to 6 km, the conductivity increases with the growth of the radioactivity level. The aerosol number density increase leads to decrease of conductivity due to loss of the light ions caused by their adhesion to aerosols. The calculations showed significant current densities at the altitude up to 12–14 km with maximum at 1–2 km. External current decreases with growth of atmospheric radioactivity.

3.3.4 Results of the Electric Field Calculation

Let us consider the electric field generation by external currents associated with the charged aerosol dynamics in the lower atmosphere. We accept the large-scale axially symmetrical external current distribution. Such distribution corresponds to vertical transport of aqueous aerosols in typhoon regions [30]. The horizontal electric field component in the ionosphere $E_r(r,\varphi) = \sqrt{E_x^2 + E_y^2}$ is calculated for various $\varphi = \arctan(y/x)$ angles, $\varphi = 0$ and corresponds to the magnetic meridian plane. The external current is induced by vertical atmospheric convection, which acts as an electrostatic generator. Air moving upward transfers small positively charged particles, whereas gravitational sedimentation transfers negative charges downward. The index of charge separation in unit cloud volume is $dQ/dt \approx 1$ C/km^{3}min $\approx 10^{-11}$ C/m^{3}s. Perhaps, the vertical convective movements in typhoon regions are characterized by smaller indices; their values are not exactly known. We assume that, at altitudes of $z_0 = 10$ km, the mean charge separation index is of $\sim 4 \times 10^{-12}$ C/m^3 s. The estimates then give the current density $j_{e0} \sim (dQ/dt)z_0 \sim 4 \times 10^{-6}$ A/m^2. It was found that the electric field component in the magnetic meridian plane is much smaller than the component in the perpendicular plane. The distribution substantially depends on the field tilt angle α. The spatial field structure has two maxima with a very small component in the magnetic meridian plane (in the center of a typhoon) for small ($<20°$) field tilt angle [30].

Seismic and volcanic activities initiate the enhanced injection of charged aerosols with soil gases into the atmosphere. These aerosol fluxes as we discussed above generate the external electric currents and related electric field perturbations. Sorokin et al. [168] have calculated the structure of such perturbations for the seismic event with axially symmetric horizontal distribution of external currents $\sim$100 km in radius. Figure 3.3 presents the distributions of a vertical component of the electric field on the Earth's surface and of the horizontal electric field component in the ionosphere. It is seen from this figure that the ionospheric field can reach the values up to 10 mV/m, whereas the vertical field component on the Earth's surface does not exceed 100 V/m. This is good illustration of the feedback mechanism for limitation of the ground electric field considered in Section 3.3.2.

The field in the ionosphere reaches a maximum at the edge of an area covered by an external current. The vertical electric field enhancement on the Earth's surface occurs in the region, which is approximately three times larger than the horizontal scale of the external current. Within this region, the field virtually does not vary with distance.

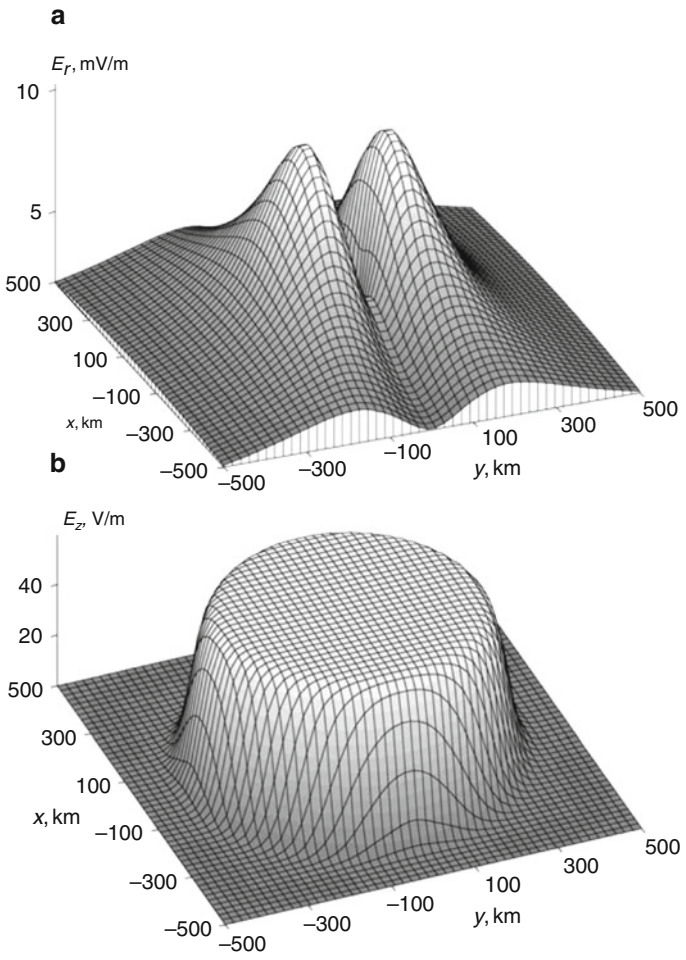

Fig. 3.3 Spatial distributions of the (**a**) horizontal electric field component in the ionosphere and (**b**) vertical field component on the Earth's surface

3.4 Plasma and Electromagnetic Effects of Seismic-Related Electric Field in the Ionosphere

3.4.1 Instability of Acoustic-Gravity Waves and the Formation of Horizontal Conductivity Inhomogeneities in the Lower Ionosphere

Growth of the electric field leads to the instability of acoustic-gravity waves in the ionosphere [172, 173]. The instability is connected with the transformation of Joule heat of the ionosphere currents into the wave energy. According to [174], the

ionosphere can be treated as a continuous medium with tensor conductivity in the low-frequency approximation. The propagation of acoustic-gravity waves in this medium is accompanied by the perturbation of conductivity and, therefore, of currents. Under certain conditions, these perturbations are sufficiently strong for Joule heat of the perturbed currents to increase an amplitude of acoustic-gravity waves. The source of energy for this instability is the electromotive force of external electric field. Field energy transforms into the energy of waves without disturbing the heat balance of the medium. Let us analyze the stability of acoustic-gravity waves in the presence of an external electric field on the assumption that the magnetic field B is directed along the z-axis, and the electric field E, along the x-axis. We shall use the equations of motion, continuity, conservation, and ideal gas state in the gravitational field g. The gas is characterized by the velocity v, density ρ, pressure p, and temperature T. We shall also use the Ohm's law for the current density j in the ionosphere.

Let us consider the horizontal propagation of a plane wave along the x-axis in a homogeneous medium, when the free fall acceleration can be neglected. We assume that the unknown values depend on the coordinates and time as $\exp(-i\omega t + ikx)$. The dispersion equation then takes the form [172]:

$$k^2 = \frac{\omega(\omega + i\omega_m)[\omega + i(\omega_m - \omega_2)]}{a^2[\omega + (\omega_m + \omega_1)]};$$
$$\omega_1 = (2\alpha + 1)(\gamma - 1)\sigma_{P0}E^2/2a^2\rho_0; \quad \omega_2 = \gamma(\gamma - 1)\sigma_{P0}E^2/2a^2\rho_0;$$
$$\omega_m = \sigma_{P0}B^2/c^2\rho_0; \quad a^2 = \gamma RT_0$$

where γ is the ratio between the specific heat capacities, R is the universal gas constant, and σ_{P0} is the Pedersen conductivity of the unperturbed ionosphere. The α coefficient characterizes the ratio between the relative changes in density of ions and gas density in the wave. The time dependence of perturbation is defined by complex frequencies. If $\omega = \omega' + i\Gamma$, where $\Gamma \ll \omega'$, one obtains $\omega' = ak$ and $\Gamma = -(\omega_m - \omega_1 - \omega_2)/2$. If $\omega_m > \omega_1 + \omega_2$, then $\Gamma < 0$, and the wave turns damp. At $\omega_1 = \omega_2 = 0$, the damping of the wave is determined by the parameter $\omega_m = \sigma_{P0}B^2/c^2\rho_0$, which characterizes induction deceleration. If $\omega_m < \omega_1 + \omega_2$, we have $\Gamma > 0$, that corresponds to instability. The equality $\omega_m = \omega_1 + \omega_2$ defines the critical field value,

$$E_k = \frac{aB}{c}\sqrt{\frac{2}{(\gamma - 1)(2\alpha + \gamma + 1)}}.$$

If the field is lower than critical, the initial perturbation fades out, and if it is higher, the wave amplification occurs. Estimation gives E_k=(7 − 8)mV/m. For the estimates we used a = 3×10^2m/s; B = 0.3Oe; c = 3×10^8m/s; $\gamma = 1.4$; $\alpha = 2$.

Let us consider the horizontal propagation of an acoustic-gravity wave (AGW) along the x-axis on the assumption that $\partial/\partial z = 0$. The dispersion equation then takes the form [172]:

$$\left(\frac{ak}{\omega}\right)^2 = \frac{(\omega + i\omega_m)\left\{\omega^2[\omega + i(\omega_m - \omega_2)] - (\omega + i\omega_m)\omega_a^2 + i\omega_2\omega_3^2\right\}}{\omega\left\{\omega^2[\omega + i(\omega_m + \omega_1)] - (\omega + i\omega_m)\omega_g^2\right\}},$$

where $\omega_a^2 = \gamma g/4H$ is the boundary acoustic frequency, $\omega_g^2 = (\gamma - 1)g/\gamma H$ is the Brunt–Vaisala frequency, and $\omega_3^2 = \omega_a^2(2\alpha + 3)/\gamma$. Let us introduce the complex refractive index $n + i\kappa = ka/\omega$. The $n = n(\omega)$ and $\kappa = \kappa(\omega)$ dependences have been calculated from this equation in the vicinity of ω_g. It appeared that the absorption coefficient is negative and has a maximum at the frequencies $\omega \sim \omega_g$. This means the instability regime, which provides the exponential growth of acoustic-gravity waves at $\omega \sim \omega_g$ and produces the periodic plasma structure. Along with density and pressure oscillations, the conductivity oscillations occur in the wave. Thus the AGW instability leads to formation of periodic horizontal inhomogeneities of the ionosphere conductivity with the characteristic scale $l \sim \lambda/2$, where λ is the wavelength at $\omega \sim \omega_g$, where the AGW growth rate is maximum. At these frequencies, the refractive index $n(\omega_g)$ reaches a maximum and the phase velocity becomes less than the velocity of sound, $v_g = a/n(\omega_g) < a$. The horizontal inhomogeneity scale is

$$l = \lambda/2 = \pi v_g/\omega_g = \pi a/\omega_g n(\omega_g). \tag{3.11}$$

Thus the enhancement of DC electric field causes the instability of acoustic-gravity waves and generation of horizontal conductivity inhomogenities in the lower ionosphere.

3.4.2 *The Formation of Longitudinal Currents and Plasma Inhomogeneities in the Upper Ionosphere and the Magnetosphere*

Horizontal conductivity inhomogeneities in the lower ionosphere change the structure of the electric fields and form the magnetic field-aligned plasma layers in the upper ionosphere [172, 173, 175]. A high conductivity along magnetic field lines results in electric field propagation into the upper ionosphere and the magnetosphere. This causes the formation of an electric circuit, which includes the longitudinal currents in the magnetosphere that transfer the electric field along geomagnetic field lines and the transverse closure currents provided by Pedersen conductivity in the ionosphere. Note that the longitudinal currents are carried by electrons, whereas ions are transverse current carriers. Therefore, the electric field propagation along geomagnetic field lines and the formation of closure currents should be accompanied by local changes in plasma density. Thus, the alternation of ionospheric E-layer conductivity in the presence of an external electric field results

in the appearance of a polarization electric field. The upward propagation of this field causes the changes in plasma density structure in the upper ionosphere. Let us estimate this effect.

Although an acoustic-gravity wave propagates along the x-axis, the conductivity inhomogeneities associated with AGW instability are extended along the y-axis. We assume that the electric field $\mathbf{E}_0$ lies in the (x, y) plane and the magnetic field $\mathbf{B}$ is directed along the z-axis. When a conductivity inhomogeneity with the amplitude $\Delta\sigma_{P,H}$ moves in the E-layer of the ionosphere as an isolated band of width $l \sim \lambda/2$ extending along the y-axis, the plasma inhomogeneity extending along the magnetic field is formed in the upper ionosphere [176]. The band moves along the x-axis with the AGW velocity $v_g = a/n(\omega_g, \omega_1)$. The magnetosphere is characterized by the Alfven velocity v_a or wave integral conductivity $\Sigma_w = c^2/4\pi v_a$. The formation of the conducting band in E-layer results in the occurrence of a polarization electric field $\Delta\mathbf{E}$, which is transferred along geomagnetic field lines into the upper ionosphere and changes the plasma density in this region. The relative magnitude of this change can be found from the equation [172]

$$\frac{N}{N_0} = \frac{1 + D_1 - v_g/v_{ex}}{1 + D_2 - v_g/v_{ex}};$$

$$D_1 = \frac{v_i E_{x0}}{\omega_i E_{y0}}; \quad D_2 = \frac{v_i}{\omega_i} \frac{(\Sigma_{P0} + \Sigma_w)E_{x0} + (\Sigma_H - \Sigma_{H0})E_{y0}}{(\Sigma_P + \Sigma_w)E_{y0}},$$

where N and N_0 are the equilibrium densities of ions inside and outside the band, $v_{ex} = -cE_{y0}/B$ is the particle drift velocity, v_g is the horizontal velocity of band movement along the x-axis, Σ_P and Σ_H are the integral conductivities of the lower ionosphere, and v_i is the ion collisions frequency. We assume that the electric field is directed along the x-axis ($E_{y0} = 0$). The equality $\Sigma_P = \Sigma_w$ holds to a fairly high accuracy in the ionosphere. If $\Delta\Sigma_P/\Sigma_{P0} = \Delta\sigma_P/\sigma_{P0}$ and $v_i cE_{x0}/\omega_i v_g B \ll 1$, the change in plasma density $\Delta N = N - N_0$ can be estimated from the equation

$$\frac{\Delta N}{N_0} = \frac{\Delta\sigma_P v_i cE_{x0}}{\sigma_{P0}\omega_i v_g B(2 + \Delta\sigma_P/\sigma_{P0})} \approx \frac{v_i cn(\omega_g)E_{x0}}{2\omega_i aB}.$$

The altitude dependence of $\Delta N/N_0$ is described by the function $v_i = v_i(z)$. Thus the appearance of horizontal inhomogeneities in the lower ionosphere conductivity results in the formation of plasma layers extended along the geomagnetic field. The transverse size of these layers coincides with the scale of horizontal spatial structure of conductivity.

3.4.3 Electromagnetic Perturbations in ULF/ELF Ranges

As mentioned above, satellite data on intensification of extremely low-frequency (ELF) radiation over earthquake region were reported repeatedly. Several

mechanisms of the generation of such radiation have been discussed during the past years (e.g., see [177]). Calculations showed that these mechanisms produced much weaker effects than those observed experimentally over the spectral range covering several hundred hertz. A new mechanism based on the transformation of atmospheric ELF noise on the small-scale inhomogeneities in the ionosphere was proposed by [36]. This pulse electromagnetic noise is generated by lightning and always exists in the Earth–ionosphere waveguide. The excitation of small-scale plasma inhomogeneities in the ionosphere before earthquake was experimentally confirmed [32] and explained by AGW instability in the presence of an overcritical DC electric field [172, 173].

Let us consider the mechanism suggested by Borisov et al. [36]. The lowest eigenmode of subionosphere waveguide (the TM mode) has the weakest attenuation at frequencies below 1 kHz and can therefore propagate through large distances. Because of the high conductivity of the Earth near the surface, the electric field of this mode is directed vertically. A horizontal electric field component appears as the altitude increases. Its value approaches the amplitude of the vertical component over the spectral range 100–1,000 Hz at altitudes of 115–120 km, at which the conductivity of the ionosphere is maximum. Horizontal components of the electric field pulses from lightning discharges induce polarization currents on the conductivity inhomogeneities. The radiation from these currents, which depends on frequency, propagates in a whistler mode upward into the upper ionosphere and the magnetosphere. Satellite should observe this radiation at the same geomagnetic field lines where plasma density inhomogenities are observed. The spectral characteristics and the intensity of this radiation were found to be near the experimentally observed values [32].

Generation of small-scale plasma density irregularities in the ionosphere over seismic zone, and the effects of these irregularities upon characteristics of very low-frequency transmitter signals propagated through these disturbances and then registered onboard a satellite were analyzed in [178]. The main effect is in observable spectral broadening of signals. The calculations showed two characteristic spatial scales of plasma density irregularities across the magnetic field. The first is 4–40 km, which has been confirmed by satellite observations, and the second is of the order or less than 100 m [18]. These smaller-size irregularities produce noticeable effect in very low-frequency signal spectral broadening, which is most pronounced when the transmitter frequency is above, but close to the local low-hybrid resonance frequency in the region where the small scale irregularities are present, which in turn sets the requirement that the transmitter frequency be in the range from 10 to 20 kHz. This corresponds to operational band of most VLF transmitters. For the 100 m irregularities, we get the spectral broadening $\sim$100 Hz that can easily be registered by simple very low-frequency receiver onboard a satellite, provided the transmitter power is high enough. This effect together with the direct satellite measurements of plasma density variations can be used as an effective tool for diagnostics of seismic-related ionospheric disturbances and therefore considered as a possible ionospheric precursor to earthquake.

The observations of ultra low-frequency electromagnetic noises in the vicinity of a forthcoming earthquake area were reported in several papers

(e.g., see [177, 179–181]). In particular, Frazer-Smith in ref. [179] have observed ULF oscillations in the frequency band 0.01–5 Hz approximately 10 days before a strong earthquake at a distance ∼50 km from the epicentre. Fitterman [56], Molchanov et al. [55], and Pilipenko et al. [57] considered a source of this phenomenon to be located in the lithosphere. An alternative ionospheric mechanism for the generation of ULF magnetic field oscillations based on excitation of gyrotropic waves (GW) was presented in refs. [182, 183].

Gyrotropic waves earlier observed by Sorokin and Fedorovich [59] propagate within a thin layer of the lower ionosphere in low and medium latitudes with weak attenuation at phase velocities from tens to hundreds of kilometers per second.

Some geophysical effects related to the generation and propagation of GW in the horizontally homogeneous ionosphere were considered in refs. [184, 185]. A comprehensive theory of these waves in the mid-latitude ionosphere was developed by Sorokin and Pokhotelov [186].

Let us consider the generation mechanism for gyrotropic waves suggested in ref. [183] where the key role, as for ELF radiation, belongs to ionospheric inhomogeneities. This mechanism involves the generation of GW in the lower ionosphere by the interaction of electromagnetic noises with periodic horizontal inhomogeneities of electrical conductivity excited by the acoustic-gravity wave instability in the presence of an overcritical DC electric field. Polarization current excited on such periodic structure forms the distributed source of gyrotropic waves with horizontal spatial scale ∼10 km. These waves propagated along the ionospheric E-layer produce the magnetic field oscillations that can be observed on the ground in the frequency band ∼1–10 Hz.

The ground-based measurements yielded the detection of discrete narrow-band spectra of ULF magnetic field oscillations during seismic enhancements, volcanic eruptions, and space shuttle launches and landing [187]. It was found that the spectrum maxima in these oscillations are located at separate frequencies of ∼2, 6, 11, and 17 Hz. An attempt to explain such discrete structure in terms of gyrotropic waves was undertaken by Sorokin and Hayakawa [188] who have analyzed the generation and propagation of GW in the conducting layer of a finite thickness in the lower ionosphere in the presence of conductivity inhomogeneities. Discrete spectrum containing several lines was obtained; the position of lines depended on the thickness of the layer with Hall conductivity. The width of those spectral lines was defined by width of a spatial spectrum of ionosphere irregularities and the ratio between Pedersen and Hall conductivities. The attenuation was determined by Pedersen conductivity and a number of frequency lines depended on the dimension of source region. For instance, if conductivity irregularities with a size of ∼80 km in horizontal direction are distributed within the ionospheric region over seismic area, then the spectrum of excited pulsations consists of six spectral lines in the frequency range 1–30 Hz. Amplitude of magnetic oscillations is defined by the intensity of ionosphere irregularities, their spatial structure, and by the wave attenuation.

Irregularities of the ionosphere conductivity can influence on the propagation of ULF waves excited in the magnetosphere through the ionosphere. In ref. [189],

Sorokin et al. have shown that such irregularities could produce the screening effect on the geomagnetic pulsations penetrating through the ionosphere and decrease the amplitude of the oscillations observed on the Earth's surface. This effect should take place during night time and be more significant for higher frequencies [189].

3.4.4 *Perturbation of the Ionosphere*

The heat flux emitted by a thin conducting layer of the ionosphere in the horizontal electric field is $\sim(10^{-4} \sim 10^{-3})$ W/m^2. One of the main sources of the ionosphere heating is short-wave solar radiation ($\lambda < 102.6$ nm). The supply of heat caused by the absorption of this radiation at altitudes above 100 km is approximately several, $10^{-3}\mathrm{W}/\mathrm{m}^2$. Depending on the solar cycle, it changes several times in either direction. An estimate made in ref. [190] shows that the Joule heat of ionospheric currents over the earthquake preparation region constitutes a substantial fraction of the total heat balance of the ionosphere. Evidently this source of heat has determining action on the state of the ionosphere. Heating the ionosphere by currents increases the scale of altitude distribution of ionospheric components and, therefore, the altitude profile of $F2$ layer. Apart from the other possible mechanisms, this heating mechanism should contribute to the observed ionosphere response on the earthquake preparation processes [190]. The ionosphere is isothermal at altitudes exceeding 200 km, and there is a positive temperature gradient over the altitude range 100–200 km. Owing to heat conductivity, the presence of the temperature gradient generates a heat flux directed downward. The Joule heat source is localized in the lower ionosphere at 120–150 km. The upper ionosphere heating can then occur only if gases move in the vertical direction. Changes in the altitude distribution of ionization in the ionosphere at a given spatial inhomogeneity of the electric field on the ground were considered in ref. [191]. They assumed that the ionosphere modification was caused by plasma drift.

An increase of the electric field and current in the lower ionosphere over a seismic region leads to additional release of Joule heat that produces additional vertical flux of neutral particles and changes the ionosphere temperature [190]. Such mechanism of effecting the formation of F2 layer is realized through collisions between ions and neutral particles and an increase in the vertical scale of their altitude distribution. The modelling of seismic-related modification of the ionosphere F region performed by Sorokin and Chmyrev [190] with use of some simplifying assumptions [192] showed that heat release in the lower ionosphere increases the height of F layer maximum and decreases the concentration of electrons at this height. The altitude profiles of ion densities are also modified towards the increase in density above F layer maximum.

Along with the rearrangement of the altitude profile of plasma density in the upper ionosphere above a seismically active region, the formation of sporadic layers in the lower ionosphere has been observed [193, 194]. The critical frequency

of the sporadic E layer, f_0E_s, reached 8 $\sim$ 9 MHz in daytime. This value corresponds to a number density of electrons $\sim 10^6$ cm^{-3}. High-altitude rocket measurements in the medium-latitude ionosphere showed that electron number density in the sporadic layer was 2×10^5 cm^{-3}, and the electric field in this layer reached 10 mV/m [195]. A model of the formation of an anomalous sporadic E layer based on the effect of atmospheric electric current flowing into the ionosphere was considered in ref. [196]. This current initiates the occurrence of a longitudinal current, which flows from the ionosphere into the magnetosphere, and transverse closure current, which flows in the conducting ionosphere layer. The atmospheric current transfers ions into the ionosphere, and the longitudinal current, which balances electric charge, transfers electrons into the ionosphere. As a result, plasma density in the lower ionosphere increases [196]. The presence of metal ions in the lower ionosphere causes the appearance of a thin ($\sim$3 km) layer of enhanced electron concentration when electric current flows into the ionosphere. This layer could be recorded as a sporadic E layer.

3.4.5 Electrodynamic Model of the Atmosphere and the Ionosphere Coupling

According to the electrodynamic model [21], an enhancement of a DC electric field in the ionosphere can be caused by an increase in conductivity of the lower atmosphere due to the intense outbursts of radioactive substance from a seismic source at the preparatory stage of earthquake. Such outbursts were repeatedly observed several days or weeks before earthquake. The time dependence of radon concentration in soil gases and in natural water was investigated by Virk and Singh [25]. An intense radon burst was registered approximately a week before the earthquake. The concentration of radon then increased by factors of 2.5 and above 1.5 in gases and water, respectively. Measurements were taken at a distance of 300 km from the epicenter. According to ref. [26], the concentration of radon increased approximately fourfold 5 days prior to an earthquake. The statistical analysis of the data obtained during 3 years of observations for about 300 micro earthquakes ($M < 4$) in south-east Germany shows that 75% of the earthquakes were preceded by a substantial increase in the concentration of radon. It can be suggested that, simultaneously with radon, other radioactive elements are injected into the atmosphere. In addition, such injections should not necessarily be related to radon. The seismic-related increase in the concentration of soil aerosols containing metal ions in the atmosphere was reported in several papers (e.g., see [23, 43].

According to the considered model [21] these injection processes are responsible for the formation of external currents and enhancement of electrical conductivity in the lower atmosphere that causes an increase in the electric field in the ionosphere, as it is shown in Fig. 3.4.

Such approach finds support in the data obtained in [197] after the Chernobyl accident. It was found that intense injections of radioactive substances into the atmosphere were accompanied by changes in the phase and amplitude of VLF signals along the propagation path crossing the accident area. The VLF signal alternations were connected with the localized lower ionosphere perturbation, which could be caused by the electric field growth in this region [198].

According to modeling [21], changes in the electrophysical parameters of the lower atmosphere lead to amplification of the electric field in the ionosphere and stimulate several effects observed experimentally. As an example, we can mention the satellite observations reported in refs. [32, 40]. The data on ULF magnetic field oscillations over the frequency range (1–8) Hz and on the vertical DC electric field component obtained onboard the "Intercosmos-Bulgaria 1300" satellite 15 min before the earthquake of 01.12.1982 were discussed in ref. [40]. An increase in the electric field $\sim$ (3–7) mV/m and the appearance of ULF magnetic field oscillations with an amplitude of 3 nT were observed in two regions: above the epicenter and in the magnetically conjugated zone. COSMOS-1809 satellite measurements over Spitak earthquake region showed that intense ELF radiation was generated over the longitude range $\leq 6^\circ$ and latitude range $2\sim4^\circ$ about the epicenter [32]. The intensity of radiation was about 10 pT at the frequencies $\sim$140 Hz (in the band

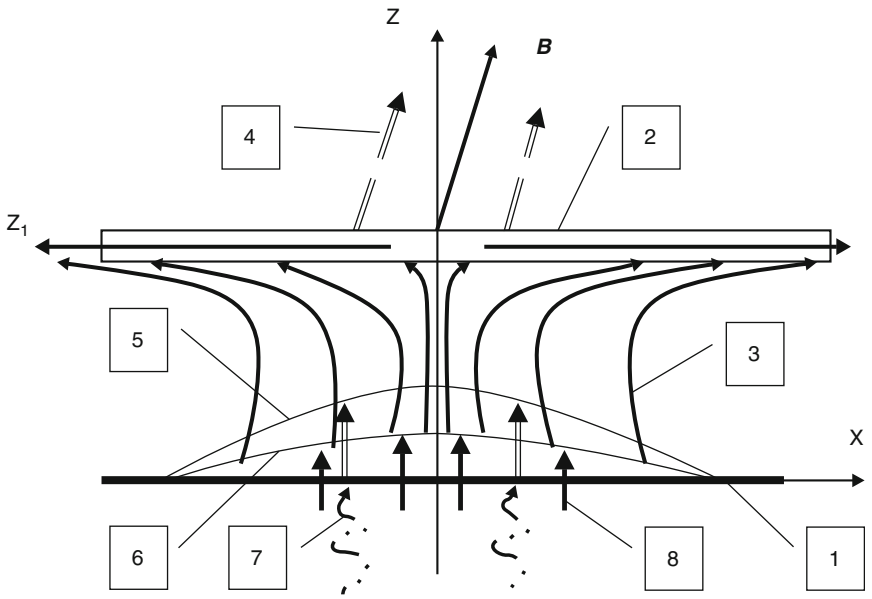

Fig. 3.4 Scheme of the model used for calculations of electric field in the atmosphere–ionosphere circuit. 1 – Earth's surface, 2 – ionosphere, 3 – conducting current in the atmosphere and the ionosphere, 4 – field aligned current, 5 – zone of upward convection of charged aerosols and external electric current formation, 6 – zone of perturbation of atmospheric conductivity induced by radioactive elements emanation, 7 – charged aerosols moving upward with soil gases, 8 – radioactive elements emanation

~25 Hz) and about 3 pT at 450 Hz(in the band ~75 Hz). In the same region, small-scale (4–10 km along the orbit) plasma density inhomogeneities with the relative amplitude (3~7)% were observed. An existence of plasma density perturbations above seismically active regions was confirmed in ref. [45].

As discussed, an increase in the ionosphere electric field above the earthquake preparation region results in the instability of acoustic-gravity waves [172, 173]. The development of this instability is accompanied by the generation of horizontal inhomogeneities in the ionosphere conductivity, whose interaction with the electric field in the ionosphere works as a source for the radiation of guided Alfven waves into the magnetosphere. These waves form the field-aligned electric currents and plasma layers extended along the geomagnetic field. The transverse spatial size of these layers coincides with the scale of the horizontal spatial structure of conductivity. Let us consider numerical estimates. At an altitude of ~1,000 km, the summed frequency of ion collisions with ions and molecules is $\nu_i \sim 0.5\ s^{-1}$ [199], and the gyrofrequency of ions is $\omega_i \sim 30\ s^{-1}$. For the velocity of sound $a = 3 \times 10^2 m/c$, perturbed electric field value $E \approx 9 mV/m$, refractive index $n \approx (1 \sim 10$ and $\omega_g \approx 2 \times 10^{-2} s^{-1}$, we obtain:

$$l = \pi a/\omega_g n(\omega_g) \approx (4 \sim 40)\ \text{km}; \quad \Delta N/N \approx (1.6 \sim 16)\%.$$

When a satellite moving at the velocity $v_s \approx 8$ km/s crosses plasma inhomogeneities of horizontal scale $l \approx (4 \sim 40)$ km, plasma density fluctuations with the period $\Delta t = l/v_s = \pi a/v_s\ \omega_g n(\omega_g) \approx (0.4 \sim 4)$ s should be observed. Since these inhomogeneities are formed by field-aligned currents, geomagnetic oscillations with the same period should be recorded when satellite crosses these currents. Their amplitude is found to be $b \sim 5$ nT. This estimate is in agreement with the satellite measurements. A scheme of such measurements is illustrated by Fig. 3.5.

Geomagnetic oscillations observed on the Earth's surface before earthquakes are interpreted in frame of the discussed model [21] in terms of gyrotropic waves (GW). These waves are connected with polarization currents associated with the horizontal inhomogeneities of conductivity and their interaction with the background electric field.

This interaction generates GW, which propagate in the horizontal direction and form geomagnetic oscillations in ULF range on the Earth's surface [182, 183]. The normalized spectrum of geomagnetic oscillations has the intensity maximum ~40% of the unperturbed (background) value and lies in ULF range. The spectral maximum frequency decreases as the horizontal scale of inhomogeneities increase. The amplitude of perturbation decreases with a distance from epicenter due to attenuation of gyrotropic waves.

According to a mechanism of electromagnetic ELF precursors to earthquakes [36], the enhanced ELF emission in the upper ionosphere arises when pulsed electromagnetic radiation from lightning discharges propagating in the Earth–ionosphere waveguide is scattered by lower ionosphere conductivity inhomogeneities over earthquake region. Intensities of lightning-induced whistler mode waves in the upper ionosphere vary substantially depending on lightning activity. The modeling

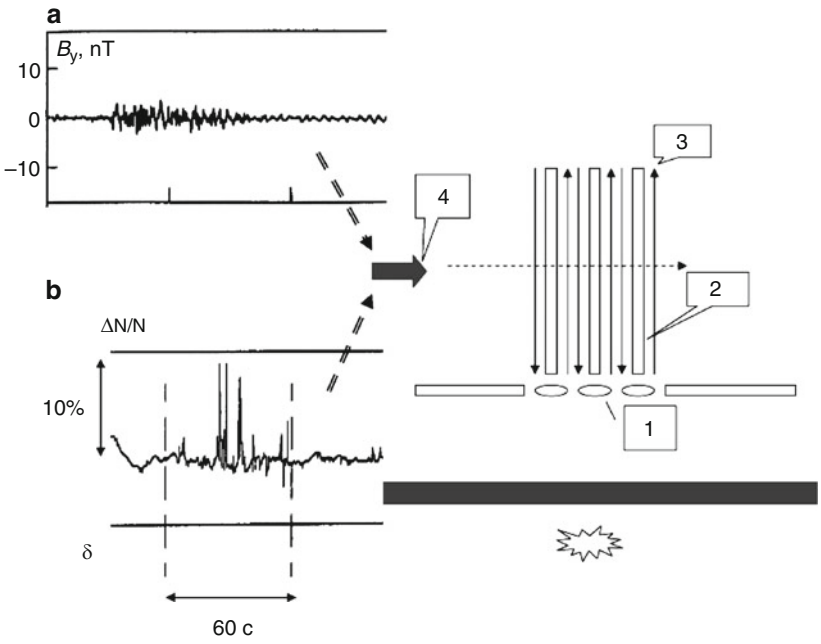

Fig. 3.5 Scheme of satellite observations of (**a**) ultralow-frequency geomagnetic field oscillations and (**b**) plasma density inhomogeneities. 1 – Horizontal ionosphere conductivity inhomogeneities, 2 – plasma density inhomogeneities stretched along the geomagnetic field, 3 – field aligned electric currents, and 4 – satellite

yields the maximum of magnetic field amplitude of ELF emission borne in this scattering process of the order of $b \approx (1 \sim 2)$ pT over the frequency range $(200 \sim 500)$ Hz. These characteristics are in agreement with the experimental data [31, 32, 200].

The estimates of the characteristic transverse size (∼10 km) and the magnitude of plasma layer density inhomogeneities obtained earlier have allowed to suppose that small-scale plasma structures excited this way could play a role of ducts or waveguides that canalized whistler mode waves along the geomagnetic field [201]. An appearance of such structures in the ionosphere above the epicenter region could increase the probability of the emergence of magnetospheric whistlers into the Earth–ionosphere waveguide and change the dispersion characteristics of signals recorded on the Earth's surface. An influence of seismic activity on the parameters of magnetospheric whistlers was reported in ref. [202]. The statistical analysis carried out demonstrated the unusual changes in mid-latitude whistler characteristics, such as an increase in the dispersion and the occurrence rate, associated with enhancement of seismic activity. Hayakawa et al. [202] discussed the possible mechanisms of such influence. In particular, they considered the seismic effect on the wave trapping in duct (or excitation of duct) at its entrance and the enhanced occurrence of ducts in the ionosphere disturbed by the acoustic or internal gravity

waves generated by earthquakes. This idea was experimentally confirmed by satellite observations of small-scale plasma density irregularities and correlated ELF emissions over the seismic zone [32].

At the preparatory stage of earthquake, large-scale changes in the ionosphere parameters were observed several days before the main seismic shock using the topside ionosphere sounding from the INTERCOSMOS-19 satellite [43]. It was shown that the altitude of F2 layer maximum increased from approximately 280 to 360 km, and the maximum electron density decreased from 3×10^5 to 10^5 cm^{-3} 1 day before the earthquake.

It was shown in Section 3.4.4 that an enhancement of the electric field and related release of Joule heat in the lower ionosphere increased the temperature and the upward mass flux in the upper ionosphere. This modifies the diffusion process that forms ionospheric F layer and changes its characteristics [190]. Let us estimate the energy flux and the temperature variation in the ionosphere caused by electric field enhancement. Assuming that the heat flux produced by solar radiation is $q_0 = 10^{-3}\mathrm{W}/\mathrm{m}^2$, and the integral Pedersen conductivity and the ionosphere electric field value to be equal to $\Sigma_\mathrm{P} \approx 10\ \Omega^{-1}$ and $E_0 \approx 3\mathrm{mV}/\mathrm{m}$, respectively, we obtain the heat flux $q = 10^{-3}\mathrm{W}/\mathrm{m}^2$. Such a flux will heat the ionosphere up to the temperature $T \approx 1,400$ K. If above the region of preparing earthquake the electric field was increased by the quantity ~6 mV/m, as observed in ref. [40], it results in the thermal flux $q = 2\ \times 10^{-3}\mathrm{W}/\mathrm{m}^2$and in the ionosphere temperature growth up to $T \approx 2{,}100$ K. This in turn leads to an elevation of the F-layer and a decrease of the maximum electron and ion densities in the layer [190] as it was observed from the INTERCOSMOS-19 satellite [43].

The other observable characteristics of the seismic-related ionosphere disturbances are ion composition and the density of the light ions. It was shown that in a near-earthquake zone during the earthquake preparation processes the H^+ and He^+ ion densities in the ionosphere increased by about a factor of 3 [44]. The modeling [190] has shown that the relative increase of the ion density (including the light ions) at altitudes 700–1,000 km could be six- to eightfold at the electric field enhancement in the ionosphere by the quantity ~6 mV/m.

In conclusion, we note that the electrodynamic model of the atmosphere and the ionosphere coupling [21] is applicable to the interpretation of some effects produced in the ionosphere by tropical storms and typhoons [29, 30, 203, 204].

3.5 Conclusions

Experimental studies and theoretical modeling show that the ionosphere is influenced by many processes, which are developed on the ground, in the lower atmosphere and in the stratosphere. This influence provides the ionosphere response to such phenomena as earthquakes, volcano eruptions, typhoons, some types of technogenic disasters, etc. The mechanisms of influencing include a set of rather complicated chemical, electrophysical, hydrodynamic and electromagnetic processes in the

atmosphere that accompany the development of these phenomena. The most comprehensive model of the atmosphere and the ionosphere coupling [21], which is presented above describes the complete causal-sequence chain of seismic-induced processes beginning from modification of the lower atmosphere state to excitation of the plasma density variations, the geomagnetic field-aligned currents and ULF/ELF emissions in the ionosphere, an elevation of the F-layer maximum, a decrease of electron density in the maximum of this layer, and a growth of light ion density in the upper ionosphere. The lower atmosphere modification is produced by the injection and turbulent transfer of charged aerosols and radioactive substances, which lead to the formation of external electric current in the atmosphere, changes in the Earth–-ionosphere electric circuit, an enhancement of DC electric field in the lower ionosphere, and related development of acoustic-gravity wave instability responsible for generation of the plasma density and electric conductivity inhomogeneities. The scattering of electromagnetic radiation from lightning by these inhomogeneities produces additional ELF wave flux observed over an earthquake area in the upper ionosphere together with plasma density irregularities.

Two other noticeable effects of the lower ionosphere modification by DC electric field enhancement are the amplitude and phase perturbations of subionospheric VLF signals and the generation of narrow band gyrotropic waves that can be observed on the Earth surface as ULF geomagnetic oscillations.

An intensified inflow of atmospheric conductivity current into the ionosphere changes the plasma density distribution in the lower ionosphere and causes the formation of an anomalous sporadic E-layer.

Let us note that the considered model is applicable to interpretation of some effects produced on the ionosphere by intense atmospheric disturbances connected with tropical storms, typhoons, etc.

In spite of definite progress in experimental studies of man-made and natural effects on the ionosphere, there is significant gap in the understanding of an origin and interconnection of many processes involved in the lithosphere–atmosphere–ionosphere coupling. The way of filing this gap is the development and implementation of long-term international research program based on coordinated observations from the ground networks, aviation, and satellite platforms of all the processes occurred in different layers of near-Earth space in association with catastrophic natural phenomena such as earthquakes, volcano eruptions, typhoons, etc.

References

1. Getmantsev, C.G., Zuikov, N.A., Kotik, D.S., Mironenko, L.F., Mityakov, N.A., Rapoport, V.O., Sazonov, Y.A., Trakhtengerts, V.Y., Eidman, V.Y.: Combination frequencies in the interaction between high-power short-wave radiation and ionospheric plasma. JETP Lett. **20**, 101–112 (1974)
2. James, H., Inan, U.S., Rietveld, M.T.: Observation on the DE-1 spacecraft of ELF/VLF waves generated by an ionospheric heater. J. Geophys. Res. **95**, 12187 (1990)

3. Inan, U.S., Golkowski, M., Carpenter, D.L., Reddell, N., Moore, R.C., Bell, T.F., Paschal, E., Kossey, P., Kennedy, E., Meth, S.Z.: Multi-hop whistler-mode ELF/VLF signals and triggered emissions excited by the HAARP HF heater. Geophys. Res. Lett. **31**, L24805 (2004)
4. Moore, R.C., Inan, U.S., Bell, T.F., Kennedy, E.J.: ELF waves generated by modulated HF heating of the auroral electrojet and observed at a ground distance of 4400 km. J. Geophys. Res. **112**, A05309 (2007). doi:10.1029/2006JA012063
5. Parrot, M., Sauvaud, J.A., Berthelier, J.J., Lebreton, J.P.: First in-situ observations of strong ionospheric perturbations generated by powerful VLF transmitter. Geophys. Res. Lett. **34**, L11111 (2007). doi:10.1029/2007GL029368
6. Frolov, V., Rapoport, V., Komrakov, G., Belov, A., Markov, G., Parrot, M., Rauch, J., Mishin, E.: Density ducts formed by heating the Earth's ionosphere with high-power HF transmitter. JETP Lett. **88**, 790–794 (2008)
7. Milikh, G.M., Papadopoulos, K., Shroff, H., Chang, C.L., Wallace, T., Mishin, E.V., Parrot, M., Berthelier, J.J.: Formation of artificial ionospheric ducts. Geophys. Res. Lett. **35**, L17104 (2008). doi:10.1029/2008GL034630
8. Dzhordzhio, N.V., Mogilevskii, M.M., Chmyrev, V.M., Kovrazhkin, R.A., Molchanov, O.A., Galperin, YuI, Boske, J.M., Roche, J.L.: Acceleration of ions in the plasma environment of the Earth by the radiation from a low-frequency transmitter on the ground. JETP Lett. **46**, 405–409 (1987)
9. Chmyrev, V.M., Kuzmin, A.K., Lazarev, V.I., Isaev, N.V., Bilichenko, S.V., Taranenko, YuN, Teltsov, M.V., Teodosiev, D.K.: Correlation of stable red arcs and H_β emissions with ion fluxes, electric fields and VLF radiation. Geom. Aeron. **28**, 813–819 (1988)
10. Chmyrev, V.M., Mogilevsky, M.M., Molchanov, O.A., Sobolev, Ya.P., Titova, E.E., Yakhnina, T.A., Suncheleev, R.N., Gladyshev, V.A., Baranets, N.V., Dzhordzhio, N.V., Galperin, Yu.I., Streltsov, A.V.: Parametric excitation of ELF waves and acceleration of ions at the injection of strong VLF waves into the ionosphere. Kosmich. Issled. **27**, 248–257 (1989)
11. Bernhardt, P.A., Scales, W.A., Grach, S.M., Keroshtin, A.N., Kotik, D.S., Polyakov, S.M.: Excitation of artificial airglow by high-power radio waves from "SURA" ionospheric heating facility. Geophys. Res. Lett. **18**(8), 1477–1480 (1991)
12. Cohen, D., Weiber, J., King, J., Kemper, S., Stephens, S., Davis, L., Spanjer, G., Winter, J., Adler, A., Easley, S., Tolliver, M., Guarnieri, J.: The SSTE-4: DSX flight experiment: design of a low-cost, R&D space mission with responsive enabling technologies. Paper N.2005-3004, AIAA 3rd Responsive Space Conference 2005, Los Angeles, CA (2005)
13. Gamble, R.J., Rodger, C.J., Clivlend, M.A., Sauvaud, J.-A., Thomson, N.R., Stewart, S.L., McCornick, R.J., Parrot, M., Berthelier, L.-J.: Radiation belt precipitation by manmade VLF transmission. J. Geophys. Res. (2008). doi:10.1029/2008JA013369
14. Molchanov, O.A.: Wave and plasma phenomena inside the ionosphere and the magnetosphere associated with earthquakes. In: Stone, W.R. (ed.) Review of Radio Science 1990–1992, pp. 591–600. Oxford University Press, New York (1993)
15. Buchachenko, A.L., Oraevskii, V.N., Pokhotelov, O.A., Sorokin, V.M., Strakhov, V.N., Chmyrev, V.M.: Ionospheric precursors to earthquakes. Phys.-Usp. **39**, 959–965 (1996)
16. Varotsos, P.: A review and analysis of electromagnetic precursory phenomena. Acta Geophys. Pol. **49**, 1–42 (2001)
17. Hayakawa, M., Molchanov, O.: Seismo-Electromagnetics (Lithosphere–Atmosphere–Ionosphere Coupling), pp. 1–477. Terrapub, Tokyo (2002)
18. Parrot, M., Berthelier, J.J., Lebreton, J.P., Sauvaud, J.A., Santolik, O., Blecki, J.: Examples of unusual ionospheric observations made by the DEMETER satellite over seismic regions. Phys. Chem. Earth **31**, 486–495 (2006)
19. Parrot, M., Berthelier, J.J., Lebreton, J.P., Treumann, R., Rauch, J.L.: DEMETER observation of EM emissions related to thunderstorms. Space Sci. Rev. **137**, 511519 (2008). doi: 10.1007/s11214-008-9347-y

20. Bhattacharya, S., Sarkar, S., Gwal, A.K., Parrot, M.: Satellite and ground-based ULF/ELF emissions observed before Gujarat earthquake in March 2006. Curr. Sci. **93**, 41–46 (2006)
21. Sorokin, V.M., Chmyrev, V.M., Yaschenko, A.K.: Electrodynamic model of the lower atmosphere and the ionosphere coupling. J. Atmos. Solar-Terr. Phys. **63**, 1681–1691 (2001)
22. Sorokin, V.M.: Plasma and electromagnetic effects in the ionosphere related to the dynamic of charged aerosols in the lower atmosphere. Russ. J. Phys. Chem. **1**, 138–170 (2007)
23. Alekseev, V.A., Alekseeva, N.G.: Investigation of metal transfer in the biosphere during gaseous emission in zones of tectonic activity using methods of nuclear physics. Nucl. Geophys. **6**, 99–105 (1992)
24. Voitov, G.I., Dobrovolsky, I.P.: Chemical and isotope – carbonic instability of the soil gases in the seismic regions. Izvestiya AN SSSR. Fizika Zemli **3**, 20–27 (1994)
25. Virk, H.S., Singh, B.: Radon recording of Uttarkashi earthquake. Geophys. Res. Lett. **21**, 737–741 (1994)
26. Heincke, J., Koch, U., Martinelli, G.: CO_2 and Radon measurements in the Vogtland area (Germany) – a contribution to earthquake prediction research. Geophys. Res. Lett. **22**, 774–779 (1995)
27. Igarashi, G., Saeki, T., Takahata, N., Sano, Y., Sumikawa, K., Tasaka, S., Sasaki, Y., Takahashi, M.: Groundwater radon anomaly before the Kobe earthquake. Science **269**, 60–61 (1995)
28. Pulinets, S.A., Alekseev, V.A., Legenka, A.D., Khegai, V.V.: Radon and metallic aerosols emanation before strong earthquakes and their role in atmosphere and ionosphere modification. Adv. Space Res. **20**, 2173–2176 (1997)
29. Isaev, N.V., Sorokin, V.M., Chmyrev, V.M., Serebryakova, O.N., Ovcharenko, O.Ya.: Electric field enhancement in the ionosphere above tropical storm region. In.: Hayakawa, M., Molchanov, O.A. (eds.) Seismo electromagnetics: litosphere–atmosphere–ionosphere coupling, pp. 313–315. Terrapub, Tokyo (2002)
30. Sorokin, V.M., Isaev, N.V., Yaschenko, A.K, Chmyrev, V.M., Hayakawa, M.: Strong DC electric field formation in the low latitude ionosphere over typhoons. J. Atmos. Solar-Terr. Phys. **67**, 1269–1279 (2005)
31. Serebryakova, O.N., Bilichenko, S.V., Chmyrev, V.M., Parrot, M., Rauch, J.L., Lefeuvre, F., Pokhotelov, O.A.: Electromagnetic ELF radiation from earthquake regions as observed by low-altitude satellites. Geophys. Res. Lett. **19**, 91–94 (1992)
32. Chmyrev, V.M., Isaev, N.V., Serebryakova, O.N., Sorokin, V.M., Sobolev, Ya.P.: Small-scale plasma inhomogeneities and correlated ELF emissions in the ionosphere over an earthquake region. J. Atmos. Solar-Terr. Phys. **59**, 967–973 (1997)
33. Gokhberg, M.B., Morgunov, V.A., Yoshino, T., Tomizawa, I.: Experimental measurements of electromagnetic emissions possibly related to earthquake in Japan. J. Geophys. Res. **87**, 7824–7828 (1982)
34. Koons, H.C., Roeder, J.L.: A comparison of ULF/ELF measurements associated with earthquakes. In: Hayakawa, M. (ed.) Atmospheric and ionospheric electromagnetic phenomena associated with earthquakes, pp. 171–175. Terrapub, Tokyo (1999)
35. Henderson, T.R., Sonwalkar, V.S., Helliwell, R.A., Inan, U.S., Fraser-Smith, A.C.: A Search for ELF/VLF emissions induced by earthquakes as observed in the ionosphere by the DE-2 satellite. J. Geophys. Res. **98**, 9503–9511 (1993)
36. Borisov, N., Chmyrev, V., Rybachek, S.: A new ionospheric mechanism of electromagnetic ELF precursors to earthquakes. J. Atmos. Solar-Terr. Phys. **63**, 3–10 (2001)
37. Kondo, G.: The variation of the atmospheric electric field at the time of earthquake. Memoirs of the Kakioka Magnetic Observatory, Kakioka. Japan **13**, 17–23 (1968)
38. Pierce, E.T.: Atmospheric electricity and earthquake prediction. Geophys. Res. Lett. **3**, 185–188 (1976)
39. Hao, J.: The anomalous of atmospheric electric field at the ground level and earthquakes. Acta Seismol. Sinica. **10**, 207–211 (1988)

40. Chmyrev, V.M., Isaev, N.V., Bilichenko, S.V., Stanev, G.A.: Observation by space-borne detectors of electric fields and hydromagnetic waves in the ionosphere over on earthquake center. Phys. Earth Planet. Inter. **57**, 110–114 (1989)
41. Tate, J., Daily, W.: Evidence of electro-seismic phenomena. Phys. Earth Planet. Inter. **57**, 1–9 (1989)
42. Vershinin, E.F., Buzevich, A.V., Yumoto, K., Saita, K., Tanaka, Y.: Correlations of seismic activity with electromagnetic emissions and variations in Kamchatka region. In: Hayakawa, M. (ed.) Atmospheric and ionospheric electromagnetic phenomena associated with earthquakes, pp. 513–518. Terrapub, Tokyo (1999)
43. Pulinets, S.A., Legenka, A.D. Alekseev, V.A.: Pre-earthquakes effects and their possible mechanisms. Dusty and dirty plasmas, noise and chaos in space and in the laboratory, pp. 545–557. Plenum Publishing, New York (1994)
44. Boskova, J., Smilauer, I., Triska, P., Kudela, K.: Anomalous behaviour of plasma parameters as observed by the Intercosmos-24 satellite prior to the Iranian earthquake of 20 June 1990. Studia Geophys. Geodet. **8**, 213–220 (1994)
45. Afonin, V.V., Molchanov, O.A., Kodama, T., Hayakawa, M., Akentieva, O.A.: Statistical study of ionospheric plasma response to seismic activity: search for reliable result from satellite observations. In: Hayakawa, M. (ed.) Atmospheric and ionospheric electromagnetic phenomena associated with earthquakes, pp. 597–617. Terra Scientific Publishing Company (TERRAPUB), Tokyo (1999)
46. Pulinets, S.A., Legenka, A.D.: Spatial-temporal characteristics of the large scale disturbances of electron concentration observed in the *F*-region of the ionosphere before strong earthquake. Cosmic Res. **41**, 221–229 (2003)
47. Tronin, A.A.: Satellite thermal survey application for earthquake prediction. In.: Hayakawa, M. (ed.) Atmospheric and ionospheric electromagnetic phenomena associated with earthquakes, pp. 717–723. Terrapub, Tokyo (1999)
48. Tronin, A.A., Hayakawa, M., Molchanov, O.A.: Thermal IR satellite data application for earthquake research in Japan and China. J. Geodyn. **33**, 519–534 (2002)
49. Qiang, Z.J., Dian, C.G., Li, L.Z.: Satellite thermal infrared precursors of two moderate-strong earthquakes in Japan and impending earthquake prediction. In: Hayakawa, M. (ed.) Atmospheric and ionospheric electromagnetic phenomena associated with earthquakes, pp. 747–745. Terrapub, Tokyo (1999)
50. Tramutoli, V., Di Bello, G., Pergova, N., Piscitalli, S.: Robust satellite techniques for remote sensing of seismically active areas. Ann. Geofis. **44**, 295–312 (2001)
51. Toroshelidze, T.I., Fishkova, L.M.: Analyzes of the middle and upper atmosphere luminescence before earthquakes. DAN SSSR, Fizika Zemli. **302**, 313–319 (1986)
52. Gokhberg, M.B., Nekrasov, A.K., Shalimov, S.L.: On influence of the unstable injection of green gases to the ionosphere in seismic region. Izvestiya AN SSSR, Fizika Zemli. **8**, 52–60 (1996)
53. Draganov, A.B., Inan, U.S., Taranenko, YuN: ULF magnetic signatures at the earth surface due to ground water flow: a possible precursor to earthquakes. Geophys. Res. Lett. **18**, 1127–1131 (1991)
54. Surkov, V., Pilipenko, V.: The physics of pre-seismic electromagnetic ULF signals. In: Hayakawa, M. (ed.) Atmospheric and ionospheric electromagnetic phenomena associated with earthquakes, pp. 357–363. Terrapub, Tokyo (1999)
55. Molchanov, O.A., Hayakawa, M., Rafalsky, V.A.: Penetration characteristics of electromagnetic emissions from an underground seismic source into the atmosphere, ionosphere, and magnetosphere. J. Geophys. Res. **100**, 1691–1712 (1995)
56. Fitterman, D.V.: Theory of electrokinetic–magnetic anomalies in a faulted half-space. J. Geophys. Res. **84**, 6031–6040 (1979)
57. Pilipenko, V.A., Fedorov, E.N., Yagova, N.V., Yumoto, K.: Attempt to detect ULF electromagnetic activity preceding earthquake. In: Hayakawa, M. (ed.) Atmospheric and

ionospheric electromagnetic phenomena associated with earthquakes, pp. 203–214. Terrapub, Tokyo (1999)
58. Alperovich, L.S., Gokhberg, M.B., Sorokin, V.M., Fedorovich, G.V.: On generation of the geomagnetic variations by acoustic oscillation occurring at the time of earthquakes. Izvestiya AN SSSR, Fizika Zemli **3**, 58–68 (1979)
59. Sorokin, V.M., Fedorovich, G.V.: Propagation of the short periodic waves in the ionosphere. Izvestiya VUZov, Radiofizika. **25**, 495–507 (1982)
60. Grimalsky, V.V., Hayakawa, M., Ivchenko, V.N., Rapoport, YuG, ZAdoroznii, V.I.: Penetration of an electrostatic field from the lithosphere into the ionosphere and its effect on the D-region before earthquakes. J. Atmos. Solar-Terr. Phys. **65**, 391–407 (2003)
61. Rapoport, Y., Grimalsky, V., Hayakawa, M., Ivchenko, V., Juarez, R.D., Koshevaya, S., Gotynyan, O.: Change of ionospheric plasma parameters under the influence of electric field which has lithospheric origin and due to radon emanation. Phys. Chem. Earth **29**, 579–587 (2004)
62. Volland, H.: Atmospheric electrodynamics. Springer, New York (1984)
63. Pasko, V.P.: Dynamic coupling of quasi-electrostatic thundercloud fields to the mesosphere and lower ionosphere: sprites and jets. Ph.D. thesis, Stanford University, Stanford, CA (1996)
64. Uman, M.A.: The lightning discharge. Academic, Orlando, FL (1987)
65. Inan, U.S., Sampson, W.A., Taranenko, Y.N.: Space-time structure of lower ionospheric optical flashes and ionization changes produced by lightning EMP. Geophys. Res. Lett. **23**, 133–138 (1996)
66. Roussel-Dupre, R.A., Gurevich, A.V., Tunnell, T., Milikh, G.M.: Kinetic theory of runaway air breakdown. Phys. Rev. E **49**, 2257–2269 (1994)
67. Bell, T.F., Pasko, V.P., Inan, U.S.: Runaway electrons as a source of Red Sprites in the mesosphere. Geophys. Res. Lett. **22**, 2127–2135 (1995)
68. Helliwell, R.A., Katsufrakis, J.P., Trimpi, M.L.: Whistler-induced amplitude perturbation in VLF propagation. J. Geophys. Res. **78**, 4679–4688 (1973)
69. Carpenter, D.L., Inan, U.S., Trimpi, M.L., Helliwell, R.A., Katsufrakis, J.P.: Perturbations of subionospheric LF and MF signals due to whistler-induced electron precipitation bursts. J. Geophys. Res. **89**, 9857–9867 (1984)
70. Burgess, W.C., Inan, U.S.: The role of ducted whistlers in the precipitation loss and equilibrium flux of radiation belt electrons. J. Geophys. Res. **98**, 15643–15650 (1993)
71. Rosenberg, T.J., Helliwell, R.A., Katsufrakis, J.P.: Electron precipitation associated with discrete, very low frequency emissions. J. Geophys. Res. **76**, 8445–8456 (1971)
72. Rycroft, M.J.: Enhanced energetic electron intensities at 100 km altitude and a whistler propagation through the plasmasphere. Planet. Space Sci. **21**, 239–247 (1973)
73. Goldberg, R.J., Curtis, S.A., Barcus, J.R.: Detailed spectral structure of magnetospheric electron bursts precipitated by lightning. J. Geophys. Res. **92**, 2505–2512 (1987)
74. Voss, H.D., Imhof, W.L., Mobila, J., Gaines, E.E., Walt, M., Inan, U.S., Helliwell, R.A., Carpenter, D.L., Katsufrakis, J.P., Chang, H.C.: Lightning-induced electron precipitation. Nature **312**, 740–749 (1984)
75. Imhof, W.L., Voss, H.D., Walt, M., Gaines, E.E., Mobila, J., Datlove, D.W., Reagan, J.B.: Slot region electron precipitation by lightning. J. Geophys. Res. **91**, 8883–8892 (1986)
76. Voss, H.D., Walt, M., Imhof, W.L., Mobila, J., Inan, U.S.: Satellite observation of lightning-induced electron precipitation. J. Geophys. Res. **103**, 11725–11732 (1998)
77. Inan, U.S., Bell, T.F., Helliwell, R.A.: Nonlinear pitch angle scattering of energetic electrons by coherent VLF waves in the magnetosphere. J. Geophys. Res. **83**, 3235–3246 (1978)
78. Chang, H.C., Inan, U.S.: Lightning-induce energetic electron precipitation from the magnetosphere. J. Geophys. Res. **90**, 4531–4539 (1985)
79. Armstrong, W.C.: Recent advances from studies of the Trimpi effect. Antarctic J. **18**, 281–286 (1983)

80. Inan, U.S., Shafer, D.C., Yip, W.Y., Orville, R.E.: Subionospheric VLF signatures of nighttime *D*-region perturbations in the vicinity of lightning discharges. J. Geophys. Res. **93**, 11455–11467 (1988)
81. Inan, U.S., Rodriguez, J.V., Idone, V.P.: VLF signatures of lightning-induced heating and ionization of the nighttime D-region. Geophys. Res. Lett. **20**, 2355–2360 (1993)
82. Inan, U.S., Bell, T.F., Pasko, V.P., Sentman, D.D., Wescott, E.M., Lyons, W.A.: VLF signatures of ionospheric disturbances associated with sprites. Geophys. Res. Lett. **22**, 3461–3466 (1995)
83. Inan, U.S., Slingeland, A., Pasko, V.P., Rodriguez, J.: VLF signatures of mesospheric/lower ionospheric response to lightning discharges. J. Geophys. Res. **101**, 5219–5228 (1996)
84. Dowden, R.L., Adams, C.D.C., Brundell, J.B., Dowden, P.E.: Rapid onset, rapid decay (RORD), phase and amplitude perturbations of VLF subionospheric transmissions. J. Atmos. Terr. Phys. **56**, 1513–1521 (1994)
85. Sentman, D.D., Wescott, E.M.: Red sprites and blue jets: thunderstorm-excited optical emissions in the stratosphere, mesosphere and ionosphere. Phys. Plasmas **2**, 2514–2522 (1995)
86. Lyons, W.A.: Characteristics of luminous structures in the stratosphere above thunderstorms as imaged by low-light video. Geophys. Res. Lett. **21**, 875–881 (1994)
87. Lyons, W.A.: Low-light video observations of frequent luminous structures in the stratosphere above thunderstorms. Mon. Weather Rev. **122**, 1940–1950 (1995)
88. Lyons, W.A.: Sprite observations above the U.S. high plains in relation to their parent thunderstorm systems. J. Geophys. Res. **101**, 29641–29652 (1996)
89. Boeck, W.L., Vaughan, O.H., Blakeslee, R.J., Vonnegut, B., Brook, M., McKune, J.: Observation of lightning in the stratosphere. J. Geophys. Res. **100**, 1465–1472 (1995)
90. Rairden, R.L., Mende, S.B.: Time resolved sprite imagery. Geophys. Res. Lett. **22**, 3465–3469 (1995)
91. Winckler, J.R., Lyons, W.A., Nelson, T., Nemzek, R.J.: New high-resolution ground-based studies of cloud-ionosphere discharges over thunderstorms (CI or Sprites). J. Geophys. Res. **101**, 6997–7012 (1996)
92. Wescott, E.M., Sentman, D., Osborne, D., Hampton, D., Heavner, M.: Preliminary results from the Sprites94 aircraft campaign: 2. Blue jets. Geophys. Res. Lett. **22**, 1209–1213 (1995)
93. Boeck, W.L., Vaughan, O.H., Blakeslee, R.J., Vonnegut, B., Brook, M.: Lightning-induced brightening in the airglow layer. Geophys. Res. Lett. **19**, 99–103 (1992)
94. Fukunishi, H., Takahashi, Y., Kubota, M., Sakanoi, K., Inan, U.S., Lyons, W.A.: Lightning-induced transient luminous events in the lower ionosphere. Geophys. Res. Lett. **23**, 2157–2163 (1996)
95. Boccippio, D.J., Williams, E.R., Heckman, S.J., Lyons, W.A., Baker, I.T., Boldi, R.: Sprites, ELF transients, and positive ground strokes. Science **269**, 1088–1093 (1995)
96. Fishman, G.J., Bhat, P.N., Mallozzi, R., Horack, J.M., Koshut, T., Kouveliotou, C., Pendleton, G.N., Meegan, C.A., Wilson, R.B., Paciesas, W.S., Goodman, S.J., Christian, H.J.: Discovery of intense gamma-ray flashes of atmospheric origin. Science **264**, 1313–1319 (1994)
97. Inan, U.S., Reising, S.C., Fishman, G.J., Horack, J.M.: On the association of terrestrial gamma-ray bursts with lightning discharges and sprites. Geophys. Res. Lett. **23**, 1017–1022 (1996)
98. Holden, D.N., Munson, C.P., Devenport, J.C.: Satellite observation of transionospheric pulse pairs. Geophys. Res. Lett. **22**, 889–893 (1995)
99. Taranenko, Y.N., Inan, U.S., Bell, T.F.: Interaction with the lower ionosphere of electromagnetic pulses from lightning: heating, attachment, and ionization. Geophys. Res. Lett. **20**, 1539–1545 (1993)
100. Taranenko, Y.N., Inan, U.S., Bell, T.F.: The interaction with the lower ionosphere of electromagnetic pulses from lightning: excitation of optical emissions. Geophys. Res. Lett. **20**, 2675–2680 (1993)

101. Milikh, G.M., Papadopoulos, K., Chang, C.L.: On the physics of high altitude lightning. Geophys. Res. Lett. **22**, 85–91 (1995)
102. Rowland, H.L., Fernsler, R.F., Huba, J.D., Bernhardt, P.A.: Lightning driven EMP in the upper atmosphere. Geophys. Res. Lett. **22**, 361–367 (1995)
103. Pasko, V.P., Inan, U.S., Taranenko, Y.N., Bell, T.F.: Heating, ionization and upward discharges in the mesosphere due to intense quasi-electrostatic thunderstorm fields. Geophys. Res. Lett. **22**, 365–370 (1995)
104. Pasko, V.P., Inan, U.S., Bell, T.F.: Sprites as luminous columns of ionization produced by quasi-electrostatic thunderstorm fields. Geophys. Res. Lett. **23**, 649–655 (1996)
105. Pasko, V.P., Inan, U.S., Bell, T.F.: Blue jets produced by quasi-electrostatic pre-discharge thunderstorm fields. Geophys. Res. Lett. **23**, 301–307 (1996)
106. Pasko, V.P., Inan, U.S., Bell, T.F., Taranenko, Y.N.: Sprites produced by quasi-electrostatic heating and ionization in the lower ionosphere. J. Geophys. Res. **102**, 4529–4539 (1997)
107. Roussel-Dupre, R.A., Gurevich, A.V.: On runaway breakdown and upward propagating discharges. J. Geophys. Res. **101**, 2297–2310 (1996)
108. Taranenko, Y.N., Roussel-Dupre, R.A.: High altitude discharges and gamma-ray flashes: a manifestation of runaway air breakdown. Geophys. Res. Lett. **23**, 571–576 (1996)
109. Lehtinen, N.G., Walt, M., Inan, U.S., Bell, T.F., Pasko, V.P.: X-ray emission produced by a relativistic beam of runaway electrons accelerated by quasi-electrostatic thundercloud fields. Geophys. Res. Lett. **23**, 2645–2652 (1996)
110. Franz, R.C., Nemzek, R.J., Winckler, J.R.: Television image of a large upward electric discharge above a thunderstorm system. Science **249**, 48–54 (1990)
111. Sentman, D.D., Wescott, E.M., Osborne, D.L., Hampton, D.L., Heavner, M.J.: Preliminary results from the Sprites94 campaign: red sprites. Geophys. Res. Lett. **22**, 1205–1211 (1995)
112. Sentman, D.D., Wescot, E.M.: Observation of upper atmosphere optical flashes recorded from an aircraft. Geophys. Res. Lett. **20**, 2857–2864 (1993)
113. Sentman, D.D., Wescott, E.M.: Red sprites and blue jets. Geophysical Institute Video Production, University of Alaska, Fairbanks (1994)
114. Vaughan, O.H., Blakeslee, R.J., Boeck, W.L., Vonnegut, B., Brook, M., McKune, J.: A cloud-to-space lightning as recorded by the space shuttle payload-bay TV cameras. Mon. Weather Rev. **120**, 1459–1465 (1992)
115. Wescott, E.M., Sentman, D.D, Heavner, M.J, Hampton, D.L.: Blue starters, discharges above an intense thunderstorm over Arkansas, July 1, 1994. In: Proceedings of the EOS Transactions. AGU, 1995 Fall Meeting, 76, F104 (1995)
116. Picard, R.H., Inan, U.S., Pasko, V.P., Winick, J.R., Wintersteiner, P.P.: Infrared glow above thunderstorms. Geophys. Res. Lett. **24**, 2635–2643 (1997)
117. Parrot, M., Berthelier, J.J., Lebreton, J.P., Treumann, R., Rauch, J.L.: DEMETER observation of EM emissions related to thunderstorms. Space Sci. Rev. **137**, 511–519 (2008). doi:10.1007/s11214-008-9347-y
118. Berthelier, J.J., Malingre, M., Pfaff, R., Seran, E., Pottelette, R., Lebreton, J.P., Parrot, M.: Lightning – induced plasma turbulence and ion heating in equatorial ionospheric depletion. Nat. Geosci. (2008). doi:10.1038/ngeo109
119. Inan, U.S., Carpenter, D.L.: Lightning-induced electron precipitation events observed at L 2.4 as phase and amplitude perturbations on subionospheric VLF signals. J. Geophys. Res. **92**, 3293–3299 (1987)
120. Clilverd, M.A., Rodger, C.J., Nunn, D.: Radiation belt electron precipitation fluxes associated with lightning. J. Geophys. Res. **109**, A12208 (2004). doi:10.1029/2004JA010644
121. Inan, U.S., Piddyachiy, D., Peter, W.B., Sauvaud, J.A., Parrot, M.: DEMETER satellite observation of lightning-induced electron precipitation. Geophys. Res. Lett. **34**, L07103 (2007). doi:10.1029/2006GL029238
122. Jones, T.B., Davis, K., Wieder, B.: Observation of *D*-region modifications at low and very low frequencies. Nature **238**, 33–37 (1972)

123. Barr, R., Rietveld, M.T., Kopka, H., Stubbe, P.: Effects of heated patch of auroral ionosphere on VLF radio wave propagation. Nature **309**, 534–538 (1984)
124. Barr, R., Rietveld, M.T., Kopka, H., Stubbe, P., Nielsen, E.: Extra-low-frequency radiation from the polar electrojet antenna. Nature **317**, 155160 (1985)
125. Bell, T.F., Inan, U.S., Danielson, M., Cummer, S.: VLF signatures of ionospheric heating by HIPAS. In: Goodmaned, J.M. (ed.) Proceedings of the 1993 Ionospheric Effects Symposium, pp. 622–628. SRI International, Arlington, VA (1993)
126. Stubbe, P., Kopka, H., Rietveld, M.T., Dowden, R.L.: ELF and VLF generation by modulated heating of the current carrying lower ionosphere. J. Atmos. Terr. Phys. **44**, 1123–1128 (1982)
127. Ferrano, A.J., Lee, H.S., Allshouse, R., Carroll, K., Lunnen, R., Collins, T.: Characteristics of ionospheric ELF radiation generated by HF heating. J. Atmos. Terr. Phys. **46**, 855–863 (1984)
128. Barr, R., Stubbe, P., Rietveld, M.T., Kopka, H.: ELF and VLF signals radiated by the "polar electrojet antenna": experimental results. J. Geophys. Res. **91**, 4451–4462 (1986)
129. Barr, R., Stubbe, P., Kopka, H.: Long-range detection of VLF radiation produced by heating the auroral electrojet. Radio Sci. **26**, 871–989 (1991)
130. Papadopoulos, K., Wallace, T., McCarrick, M., Milikh, G.M., Yang, X.: On the efficiency of ELF/VLF generation using HF heating of the auroral electrojet. Plasma Phys. Rep. **29**, 561–567 (2003)
131. Pashin, A.B., Mochalov, A.A., Bosinger, T., Rietveld, M.T.: Physics of auroral phenomena. In: Proceedings of the XXVI Annual Seminar, Apatity, pp. 111–114. Kola Science Centre, Russian Academy of Science (2003)
132. Kimura, I., Stubbe, P., Rietveld, M.T., Barr, R., Ishida, K., Kasahara, Y., Yagitani, S., Nagano, I.: Collaborative experimentsby Akebono satellite, Tromso ionospheric heater, and European incoherent scatter radar. Radio Sci. **29**, 23–29 (1994)
133. Ferrano, A.J., Lee, H.S., Allshouse, R., Carroll, K., Tomko, A.A., Kelly, F.J., Joiner, R.G.: VLF/ELF radiation from the ionospheric dynamo current system modulated by powerful HF signals. J. Atmos. Terr. Phys. **44**, 1113–1119 (1982)
134. McCarrick, M.J., Sentman, D.D., Wong, A.Y., Wuerker, R.F., Chouinard, B.: Excitation of ELF waves in the Schumann resonance range by modulated HF heating of the polar electrojet. Radio Sci. **25**, 1291–1298 (1990)
135. Villasenor, J., Wong, A.Y., Song, B., Pau, J., McCarrick, M., Sentman, D.: Comparison of ELF/VLF generation modes in the ionosphere by the HIPAS heater array. Radio Sci. **31**, 211–217 (1996)
136. Kimura, I., Wong, A., Chouinard, B., McCarrick, M., Okada, T.: Satellite and ground observations of HIPAS VLF modulation. Geophys. Res. Lett. **18**, 309–314 (1991)
137. Milikh, G.M., Papadopoulos, K., McCarrick, M., Preston, J.: ELF emissions generated by the HAARP HF-heater using varying frequencies and polarization. Izvestiya VUZov, Radiofizika **42**, 728–733 (1999)
138. Platino, M., Inan, U.S., Bell, T.F., Parrot, M., Kennedy, E.J.: DEMETER observations of ELF waves injected with the HAARP HF transmitter. Geophys. Res. Lett. **33**, L16101 (2006)
139. Moore, R.C.: ELF/VLF wave generation by modulated HF heating of the auroral electrojet. Ph.D. thesis, Stanford University, Stanford, CA (2007)
140. Rapoport, V.O., Frolov, V.L., Komrakov, G.P. Markov, G.A., Belov, A.S., Parrot, M., Rauch, J.L.: Some results of measuring the characteristics of electromagnetic and plasma disturbances stimulated in the outer ionosphere by high-power high-frequency radio emission from the "Sura" facility. Radiophys. Quantum Electron. **50**, 645–651 (2007)
141. Frolov, V., Komrakov, G., Rapoport, V., Ryzhov, N., Belov, A., Markov, G., Parrot, M., Rauch, J., Reitveld, M.: Phenomena observed by HF heating of middle – and high-latitude ionosphere and registered with DEMETER instruments. Geophys. Res. Abstracts **10**, EGU 2008-A-03872 (2008a)

142. Zhulin, I.A., Lyakhov, S.B., Majorov, A.D., Managadze, G.G., Mogilevsky, M.M., Chmyrev, V.M.: Artificially stimulated electron precipitation from the Earth's magnetosphere. Dokl. Akad. Nauk SSSR **230**, 1073–1077 (1976)
143. Imhof, W.L., Reagan, J.B., Voss, H.D., Gaines, E.E., Datlowe, D.W., Mobilia, J., Helliwell, R.A., Inan, U.S., Ratsufrakis, J.P.: Direct observation of radiation belt electrons precipitated by the controlled injection of VLF signals from a ground-based transmitter. Geophys. Res. Lett. **10**, 361–366 (1983)
144. Imhof, W.L., Reagan, J.B., Voss, H.D., Gaines, E.E., Datlowe, D.W., Mobilia, J., Helliwell, R.A., Inan, U.S., Ratsufrakis, J.P.: The modulated precipitation of radiation belt electrons by controlled signals from VLF transmitter. Geophys. Res. Lett. **10**, 615–620 (1983)
145. Inan, U.S., Chang, H.C., Helliwell, R.A., Imhof, W.L., Reagan, J.B., Walt, M.: Precipitation of radiation belt electrons by man-made waves: a comparison between theory and measurement. J. Geophys. Res. **90**, 359–370 (1985)
146. Kovrazhkin, R.A., Mogilevsky, M.M., Bosqued, J.-M., Galperin, Y.I., Dzhordzhio, N.V., Lisakov, Y.V., Molchanov, O.A., Reme, A.: Observation of particle precipitation from the ring-current zone stimulated by powerful ground-based VLF transmitter. JETP Lett. **38**, 397–402 (1983)
147. Kovrazhkin, R.A., Mogilevsky, M.M., Molchanov, O.A., Galperin, Y.I., Dzhordzhio, N.V., Lisakov, Y.V., Bosqued, J.-M., Reme, A.: Direct detection of the precipitation of ring current electrons and protons stimulated by artificial VLF emission. Geophys. Res. Lett. **11**, 705–709 (1984)
148. Sauvaud, J.-A., Maggiolo, R., Jacquey, C., Parrot, M., Berthelier, J.-J., Gamble, R.J.: Radiation belt electron precipitation due to VLF transmission. Satellite observations. Geophys. Res. Lett. **35**, L09101 (2008). doi:10.1029/2008GL033194
149. Inan, U.S., Rodriguez, J.V., Lev-Tov, S., Oh, J.: Ionospheric modification with a VLF transmitter. Geophys. Res. Lett. **19**, 2071–2077 (1992)
150. Barr, R., Rietveld, M.T., Stubbe, P., Kopka, H.: The diffraction of VLF radio waves by a patch of ionosphere illuminated by a powerful HF transmitter. J. Geophys. Res. **90**, 2861–2869 (1985)
151. Taranenko, Y.N., Inan, U.S., Bell, T.F.: VLF-HF heating of the lower ionosphere and ELF wave generation. Geophys. Res. Lett. **19**, 61–66 (1992)
152. Rodriguez, J.V.: Modification of the Earth's ionosphere by very-low-frequency transmitter. Ph.D. thesis, Stanford University, Stanford, CA (1994)
153. Rodriguez, J.V., Inan, U.S.: Electron density changes in the nighttime *D* region due to heating by very-low-frequency transmitter. Geophys. Res. Lett. **21**, 93–98 (1994)
154. Likhter, Ya.I., Molchanov, O.A., Chmyrev, V.M.: Modulation of spectrum and amplitude of low-frequency signal in the magnetosphere. JETP Lett. **14**, 325–327 (1971)
155. Bell, T.F., James, H.G., Inan, U.S., Katsufrakis, J.P.: The apparent spectral broadening of VLF transmitter signals during trans-ionospheric propagation. J. Geophys. Res. **88**, 4813–4818 (1983)
156. Titova, E.E., Di, V.I., Yurov, V.E., Raspopov, O.M., Trakhtengerts, V.Y., Jiricek, F., Triska, P.: Interaction between VLF waves and turbulent ionosphere. Geophys. Res. Lett. **11**, 323–327 (1984)
157. Bell, T.F., Inan, U.S., Lauben, D., Sonwalkar, V.S., Helliwell, R.A., Sobolev, YaP, Chmyrev, V.M., Gonzalez, S.: DE-1 and COSMOS-1809 observations of lower hybrid waves excited by VLF whistler mode waves. Geophys. Res. Lett. **21**, 653–656 (1994)
158. Taranenko, YuN, Chmyrev, V.M.: Interaction between whistler waves and ion-cyclotron waves in magnetospheric plasma. Radiophys. Quant. Electron. **29**, 373–376 (1986)
159. Taranenko, YuN, Chmyrev, V.M.: Parametric interaction of whistler and electromagnetic ion-cyclotron waves in ionospheric plasma. Geom. Aeron. **29**, 459–464 (1989)
160. Chmyrev, V.M., Draganov, A.B., Taranenko, YuN, Teodosiev, D.: Acceleration of particles in the upper ionosphere and the magnetosphere due to decay interactions of whistlers, part 1. Phys. Scr. **43**, 495–502 (1991)

161. Chang, T., Crew, G.B., Hershkowtz, N., Jasper, J.R., Retterer, J.M., Winningham, J.D.: Transverse acceleration of oxygen ions by electromagnetic ion cyclotron resonance with broad band left hand polarized waves. Geophys. Res. Lett. **13**, 636–640 (1986)
162. Frazer-Smith, A.C., Cole, C.A.: Initial observations of the artificial stimulation of ULF pulsations by pulsed VLF transmissions. Geophys. Res. Lett. **2**, 146–149 (1975)
163. Chmyrev, V.M., Roldugin, V.K., Zhulin, I.A., Mogilevsky, M.M., Di, V.I., Koshelevsky, V.K., Bushmarin, V.A., Raspopov, O.M.: Artificial injection of very low-frequency (VLF) waves into the ionosphere and the magnetosphere of the Earth. JETP Lett. **23**, 409–412 (1976)
164. Chmyrev, V.M., Taranenko, Yu.N, Kopytenko, Yu.A., Voronov, P.V., Draganov, A.B.: Observation of ULF pulsations correlated with transmission of VLF waves and amplification of ULF waves by O^+ ion conics in the equatorial magnetosphere. Paper presented at AGU Chapman Conference on auroral plasma dynamics, Minneapolis, MN, 21–25 Oct 1991
165. Sorokin, V.M., Chmyrev, V.M.: Electrodynamic model of ionospheric precursors of earthquakes and certain types of disasters. Geom. Aeron. **42**, 821–830 (2002)
166. Molchanov, O.A., Hayakawa, M.: VLF transmitter earthquake precursors influenced by a change in atmospheric electric field. In: Proceedings of 10th International Conference on Atmospheric Electricity, pp. 428–431. Osaka, Japan, 10–14 June 1996
167. Boyarchuk, K.A., Lomonosov, A.M, Pulinets, S.A., Hegai, V.V.: Variability of the Earth's atmospheric electric field and ion-aerosols kinetics in the troposphere. Studia Geophys. Geod. **42**, 197–206 (1998)
168. Sorokin, V.M., Chmyrev, V.M., Yaschenko, A.K.: Theoretical model of DC electric field formation in the ionosphere stimulated by seismic activity. J. Atmos. Solar-Terr. Phys. **67**, 1259–1268 (2005)
169. Sorokin, V.M., Yaschenko, A.K.: Perturbation of the conductivity and electric field in the Earth–ionosphere layer over preparing earthquake. Geom. Aeron. **39**, 100–106 (1999)
170. Sorokin, V., Yaschenko, A.: Electric field disturbance in the Earth–ionosphere layer. Adv. Space Res. **26**, 1219–1225 (2000)
171. Sorokin, V.M., Yaschenko, A.K., Hayakawa, M.: A perturbation of DC electric field caused by light ion adhesion to aerosols during the growth in seismic-related atmospheric radioactivity. Nat. Hazards Earth Syst. Sci. **7**, 155–163 (2007)
172. Sorokin, V.M., Chmyrev, V.M., Isaev, N.V.: A generation model of mall-scale geomagnetic field-aligned plasma inhomogeneities in the ionosphere. J. Atmos. Solar-Terr. Phys. **60**, 1331–1342 (1998)
173. Sorokin, V.M., Chmyrev, V.M.: On acoustic gravity waves instability by electric field in the ionosphere. Geom. Aeron. **39**, 38–45 (1999)
174. Piddington, J.H.: The transmission of geomagnetic disturbances through the atmosphere and interplanetary space. Geophys. J. **2**, 173–189 (1959)
175. Chmyrev, V.M., Sorokin, V.M., Pokhotelov, O.A.: Theory of small scale plasma density inhomogeneities and ULF/ELF magnetic field oscillations excited in the ionosphere prior to earthquakes. In: Hayakawa, M. (ed.) Atmospheric and Ionospheric Electromagnetic Phenomena Associated with Earthquakes, pp. 759–776. Terrapub, Tokyo (1999)
176. Lyatsky, V.B., Maltsev, YuP: Magnetosphere–Ionosphere Coupling. Nauka, Moscow (1983)
177. Molchanov, O.A., Mazhaeva, O.A., Golyavin, A.N., Hayakawa, M.: Observation by Intercosmos-24 satellite of ELF–VLF electromagnetic emissions associated with earthquakes. Ann. Geophys. **11**, 431–440 (1993)
178. Chmyrev, V.M., Sorokin, V.M., Shklyar, D.R.: VLF transmitter signals as a possible tool for detection of seismic effects on the ionosphere. J. Atmos. Solar-Terr. Phys. **70**, 2053–2060 (2008)
179. Frazer-Smith, A.C., Bernardi, A., McGill, P.R., Ladd, M.E., Helliwell, R.A., Villard Jr., O.G.: Low-frequency magnetic field measurements near epicentre of the MS 7.1 Loma Prieta earthquake. Geophys. Res. Lett. **17**, 1465–1468 (1990)

180. Kopytenko, Y.A., Matiashvili, T.G., Voronov, P.M., Kopytenko, E.A., Molchanov, O.A.: Detection of ultra-low-frequency emissions connected with the Spitak earthquake and its aftershock activity, based on geomagnetic pulsations data at Dusheti and Vardzia observatories. Phys. Earth Planet. Inter. **77**, 85–89 (1993)
181. Hayakawa, M., Kawate, R., Molchanov, O.A., Yumoto, K.: Results of ultra-low-frequency magnetic field measurements during the Guam earthquake of August 1993. Geophys. Res. Lett. **23**, 241–250 (1996)
182. Sorokin, V.M., Chmyrev, V.M., Yaschenko, A.K.: Ultra low frequency oscillations of magnetic field on the Earth's surface generated by irregularities of the ionosphere conductivity. Geom. Aeron. **41**, 327–331 (2001)
183. Sorokin, V.M., Chmyrev, V.M., Yaschenko, A.K.: Ionospheric generation mechanism of geomagnetic pulsations observed on the Earth's surface before earthquake. J. Atmos. Solar-Terr. Phys. **64**, 21–29 (2003)
184. Sorokin, V.M.: Wave processes in the ionosphere related to geomagnetic field. Izvestiya VUZov, Radiofizika. **31**, 1169–1179 (1988)
185. Sorokin, V.M., Yaschenko, A.K.: Propagation of the Pi2 pulsations in the low ionosphere. Geom. Aeron. **28**, 655–660 (1988)
186. Sorokin, V.M., Pokhotelov, O.A.: Gyrotropic waves in the mid-latitude ionosphere. J. Atmos. Solar-Terr. Phys. **67**, 921–930 (2005)
187. Rauscher, E.A., Van Bise, W.I.: The relationship of extremely low frequency electromagnetic and magnetic fields associated with seismic and volcanic natural activity and artificial ionospheric disturbances. In: Hayakawa, M. (ed.) Atmospheric and Ionospheric Electromagnetic Phenomena Associated with Earthquakes, pp. 459–487. Terrapub, Tokyo (1999)
188. Sorokin V. M., Hayakawa, M.: On the generation of narrow-banded ULF/ELF pulsations in the lower ionospheric conducting layer. J. Geophys. Res. **113**, A06306 (2008). doi:10.1029/2008JA013094
189. Sorokin, V.M., Fedorov, E.N., Schekotov, AYu, Molchanov, O.A., Hayakawa, M.: Depression of the ULF geomagnetic pulsation related to ionospheric irregularities. Ann. Geophys. **47**, 191–198 (2004)
190. Sorokin, V.M., Chmyrev, V.M.: Modification of the Ionosphere by Seismic Related Electric Field. In: Hayakawa, M. (ed.) Atmospheric and ionospheric electromagnetic phenomena associated with earthquakes, pp. 805–818. Terrapub, Tokyo (1999)
191. Kim, V.P., Khegay, V.V., Nikiforova, V.V.: On possible perturbation of the night ionosphere E region over large scale tectonic fault. Izvestiya RAN, Fizika Zemli. **7**, 35–39 (1995)
192. Bowhill, S.A.: The formation of the daytime peak of the ionospheric *F*2-layer. J. Atmos. Terr. Phys. **24**, 503–520 (1962)
193. Ondoh, T., Hayakawa, M.: Seismo discharge model of anomalous sporadic *E* ionization before great earthquakes. In.: Hayakawa, M., Molchanov, O.A. (eds.) Seismo electromagnetics: litosphere–atmosphere–ionosphere coupling, pp. 385-390. Terrapub, Tokyo (2002)
194. Ondoh, T.: Anomalous sporadic-*E* layers observed before M7.2 Hyogo-ken Nanbu earthquake; Terrestrial gas emanation model. Adv. Polar Upper Atmos. Res. **17**, 96–108 (2003)
195. Yokoyama, T., Yamamoto, M., Pfaff, R.F., Fukao, S., Iwagami, N.: SEEK-2 campaign measurement of the electric field in the E-region and its association with the QP echoes. In: Abstracts for the 112th SGEPSS Fall Meeting, pp. 12–13. University of Electro-Communications, Tokyo (2002)
196. Sorokin, V.M., Yaschenko, A.K., Hayakawa, M.: Formation mechanism of the lower ionosphere disturbances by the atmosphere electric current over a seismic region. J. Atmos. Solar-Terr. Phys. **68**, 1260–1268 (2006)
197. Fuks, I.M., Shubova, R.S.: Anomaly in ELF signals as response to the low atmosphere processes. Geom. Aeron. **34**, 130–134 (1995)
198. Martynenko, S.I., Fuks, I.M., Shubova, R.S.: Ionospheric electric-field influence on the parameters of VLF signals connected with nuclear accidents and earthquakes. J. Atmos. Electr. **15**, 259–269 (1996)

199. Schunk, R.W., Nagy, A.F.: Ionospheres of terrestrial planets. Rev. Geophys. Space Phys. **18**, 813–852 (1980)
200. Parrot, M.: Statistical study of ELF/VLF emissions recorded by a low-altitude satellite during seismic events. J. Geophys. Res. **99**, 23339–23347 (1994)
201. Sorokin, V.M., Chmyrev, V.M., Hayakawa, M.: The formation of ionosphere–magnetosphere ducts over the seismic zone. Planet. Space Sci. **48**, 175–182 (2000)
202. Hayakawa, M.T., Yoshino, T., Morgounov, V.A.: On the possible influence of seismic activity on the propagation of magnetospheric whistlers at low latitudes. Phys. Earth Planet. Inter. **77**, 97–102 (1993)
203. Sorokin, V.M., Cherny, G.P.: It is quite possible to monitor typhoons from outer space. Aerospace Courier. N. 3, pp. 84–87 (1999)
204. Isaev, N.V., Sorokin, V.M., Chmyrev, V.M., Serebryakova, O.N.: DC electric fields in the ionosphere related to sea storms and typhoons. Geom. Aeron. **42**, 670–676 (2002)